Simulating the TCE DNAPL Source Zone Below the Water Table at the Santa Susanna Field Laboratory

by

Kaiying Qiu

A thesis
presented to the University of Waterloo
in fulfillment of the
thesis requirement for the degree of
Master of Science
in
Earth Sciences

Waterloo, Ontario, Canada, 2015

© Kaiying Qiu 2015

AUTHOR'S DECLARATION

I hereby declare that I am the sole author of this thesis. This is a true copy of the thesis, including any required final revisions, as accepted by my examiners.

I understand that my thesis may be made electronically available to the public.

Kaiying Qiu

Abstract

Both 2D and 3D numerical models using the CompFlow Bio were built to simulate TCE introduced from 1940 through 1990 due to industrial activities, in the fractured bedrock with a turbidities sequence of sandstones with shale interbeds underneath the Santa Susana Field Laboratory (SSFL). The domain size is 50m x 0.3m x100m and the fracture apertures are 75 and 100 microns in the 2D conceptual model; while due to computational limits, the domain size is 5m x 5m x15m and the fracture apertures are 75 ~ 150 microns in the 3D conceptual model. The bulk hydraulic conductivity estimate from 2D simulation is on the level of 10^{-7} m/s, which is less than that estimate from 3D one whose values is on the level of 10^{-6} m/s. With the rock core VOC analyses for the source zone and outflow boundary (only for 2D domain) compared with field data from SSFL, it presents that NAPL is original dominant phase of TCE in the water, and then it tends to dissolve and so as to be finally fluxed out of the domain. And by investigating the mass flux of TCE in the aqueous phase exists the fence boundary in fracture and matrix, Flow through fracture is proved to be easier than that through matrix, and larger fractures become the main conduit.

Acknowledgements

First and foremost, I acknowledge my supervisor, Dr. Andre Unger, and his PHD student, Kenneth Mark Walton, for their support and mentorship. I sincerely thank them for their dedication to this project – their commitment, guidance and timely advice have made this work possible. I acknowledge also my thesis committee members, Drs. Beth Parker, Marios Ioannidis, and Walter Illman, for their teachings, advice and editorial comments throughout this process.

Specific thanks go to: Dr. Walton for his expertise in technical support in running the numerical models using the CompFlow Bio and creating layer files with Tecplot; Dr. Unger and Dr. Illmanwho generously gave their time and thoughtful criticism for reviewing my thesis and giving valuable comments.

I gratefully acknowledge my sources of funding through this course of research: during my time as a Master's candidate, from The Boeing Company via the University Consortium for Field-Focused Groundwater Contamination Research, led by Dr. Parker and Dr. John Cherry.

Last but not least, I owe a great debt of gratitude to my parents, Jiaying Qiu and Lihua Liao who gave all their love and support to me.

Table of Contents

List of Figures

List of Tables

Chapter 1
Introduction

1.1 Santa Susanna Field Laboratory site description

The Santa Susana Field Laboratory (SSFL), is located on top of a mountain elevated about 50-380 m above the valley floor and populated urban centers in southeast of Ventura County, 20 miles northwest of downtown of Los Angeles, California (Figure 1). The mountain underneath SSFL composed of fractured Chatsworth Formation bedrock, a turbidities sequence of sandstones with shale interbeds (Figure 2). In this study, the PM is simplified to have homogeneous properties representative of Chatsworth formation sandstone The matrix hydraulic conductivity (Km) within the Chatsworth Formation is ranges from $1x10^{-11}$ cm/s to $1x10^{-3}$ cm/s with a geological mean value of $4.1x10^{-7}$(data from Hurley, 2003). Fractures at the site are typically vertical or sub-vertical joints or Parallel bedding plane fractures dipping at 25° to 30°, but we idealize as vertical or horizontal in this study (Walton, 2013). Variety of test methods for fracture apertures have been studied at this site, including Sterling, McWhorter and Reiners, and Kennel et al.; the mean hydraulic aperture lies between 90-125um based on different location and methods. As Walton did in his thesis, the fracture length is chosen in each spatial direction from uniform distribution between 2.0m and 7.0m; because less is known about fracture length at the SSFL site. The fracture density is set to be 3/m as a rough aggregation of data from Kennel et al. and Schlumberger Water Services. The fracture network disperses randomly and dominates the flow, and the bulk conductivity (Kb) distribution is ranged from $1x10^{-9}$ to $1x10^{-4}$ (m/s) according to Cherry, McWhorter et al. 2009. Groundwater is mounded in the mountain with water table about 3-20m below the ground surface, and discharges out of mountain-slope seeps or joints the regional flow system. Much of the site is in a groundwater recharge area at the tomographic high and flows down and out to hillside drainages at seeps or to adjacent valleys.

Due to industrial activities from 1940 through 1990, TCE and its daughter products were unintentionally released to surface and groundwater in the mountain at SSFL. And the TCE plumes formed in the interconnected fractures as a result of rainfall infiltration and the groundwater flow. Figure 3 is a site conceptual model that presents the key elements of the Santa Susanna Field Laboratory site conditions strongly influencing groundwater flow as well as contaminant fate and transport (Cherry et al., 2009).

TCE is toxic contaminant with low solubility in the water, and therefore, commonly migrates as an immiscible phase liquid in the subsurface and can spread/travel/invade large volumes of fractured rock. Its mobility in the both the DNAPL and aqueous phase is large and can reach groundwater or surface water receptors causing concerns with impacts to ecosystems and or human health. Therefore, management efforts can be better informed by studying their behavior including numerical modeling to assess contamination and remediation scenarios, to better assess how to best protect the groundwater resource and receptors.

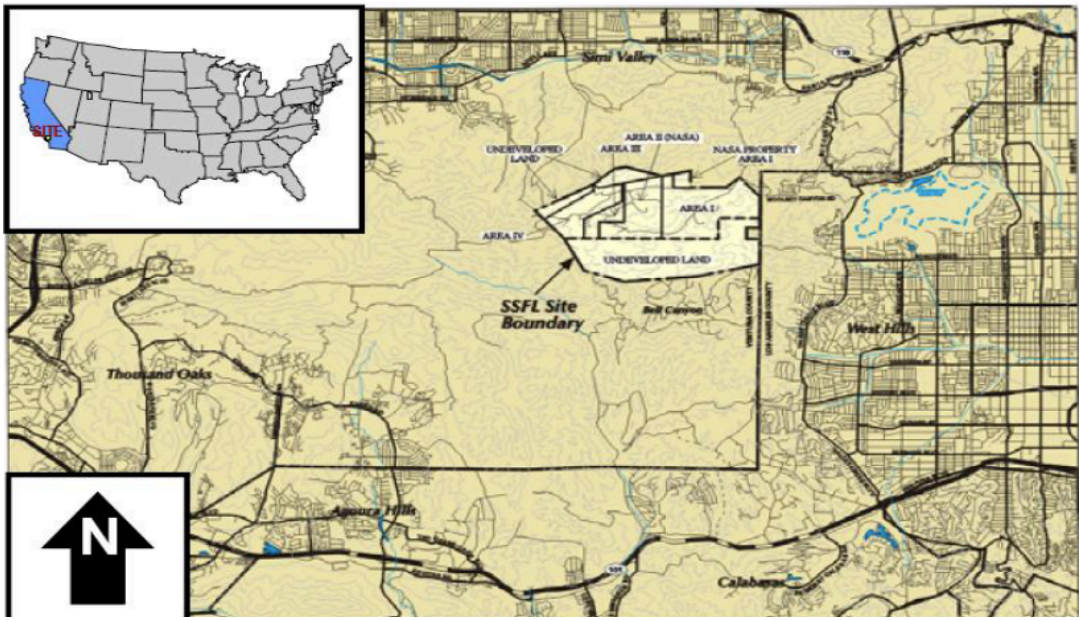

Figure 1 Regional topography and location of the Santa Susana Field Laboratory (Cherry et al. 2009)

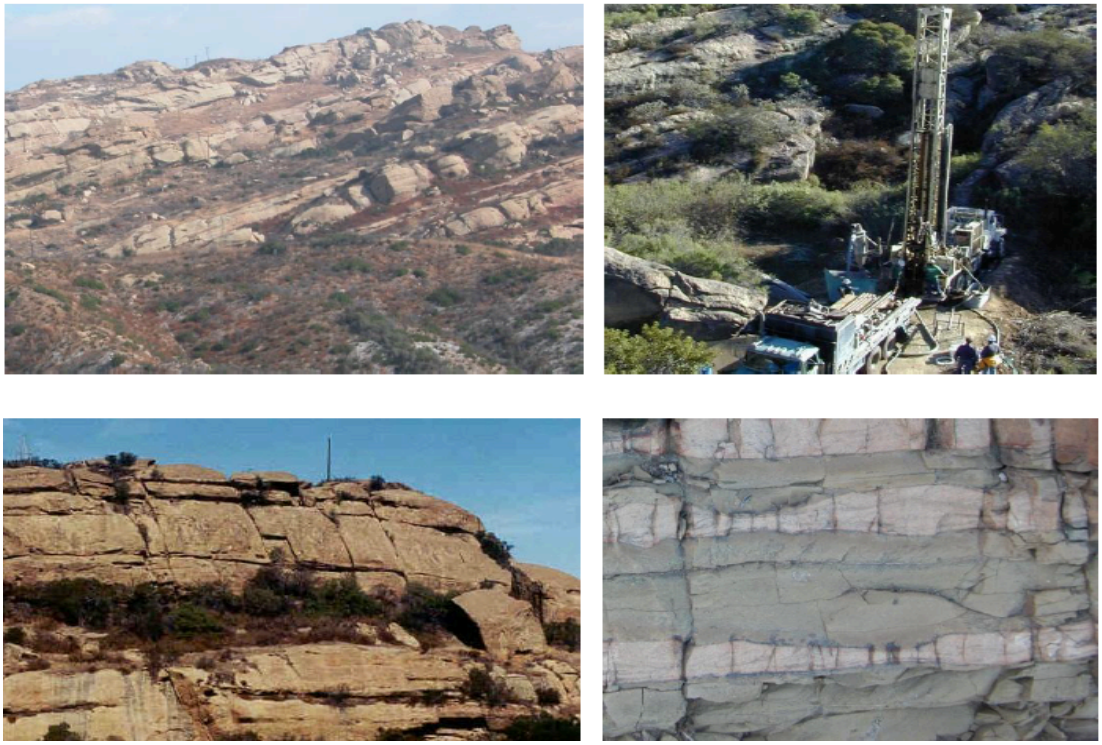

Figure 2 Pictures of site geology in the Santa Susana Field Laboratory (SSFL)(Cherry et al. 2009)

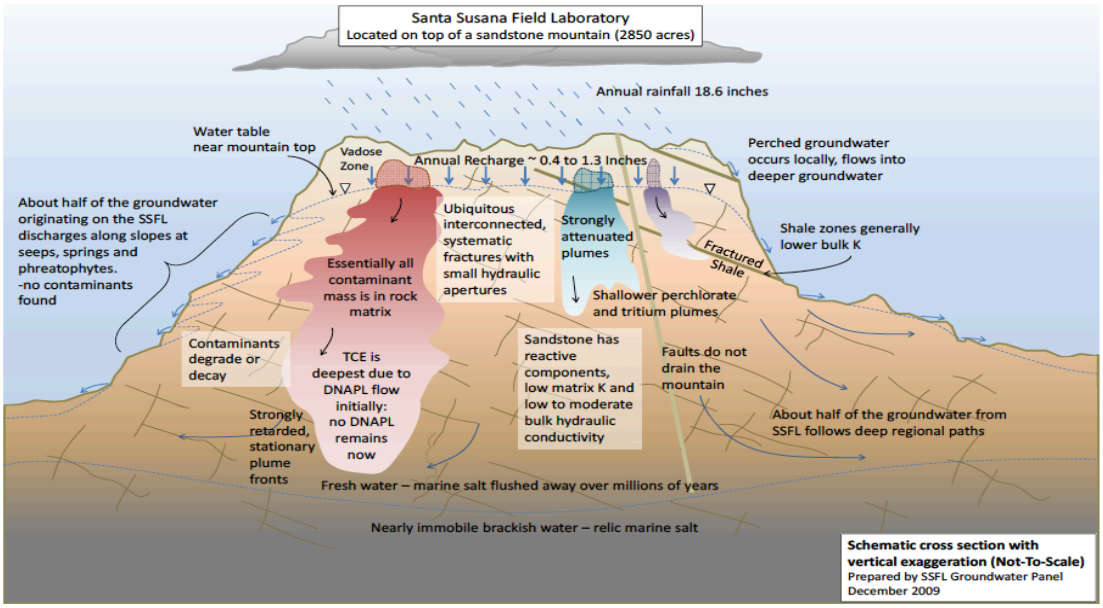

Figure 3 Schematic of SSFL Site Conceptual Model (SCM) (Cherry et al. 2009)

1.2 Source Zone and Plume Evolution Conceptual Model

Figure 4 illustrate the conceptual stages in the time evolution of source zone and plume at chlorinated solvent DNAPL sites on fractured porous sedimentary rock first presented by Parker et al. 1994 & 1997. DNAPL flows in fracture network soon after it is input to the rock, and begins to dissolve and diffuse into rock matrix. As time goes on, all DNAPL mass will completely dissolved and the contaminant mass now exists almost entirely in the rock matrix as dissolved and sorbed mass due to diffusion driven mass transfer. At this stage, there is no distinct difference in contaminant state between the zone initially referred to as the source zone and the plume, since the source zone no longer has DNAPL. An Example (Figure 5) of rock core analysis results for TCE in sandstone at a location near TCE DNAPL source zone in the Simi Hill in Ventura County, California shows that all analyses are much below TCE solubility indicating lack of DNAPL presence. Due to lateral groundwater flow, complete mass translocate very slowly from much of the initial source zone volume into the down gradient plume, and the plume front is migrating only slowly or is stable or shrinking due to the combined effects of matrix diffusion and degradation.

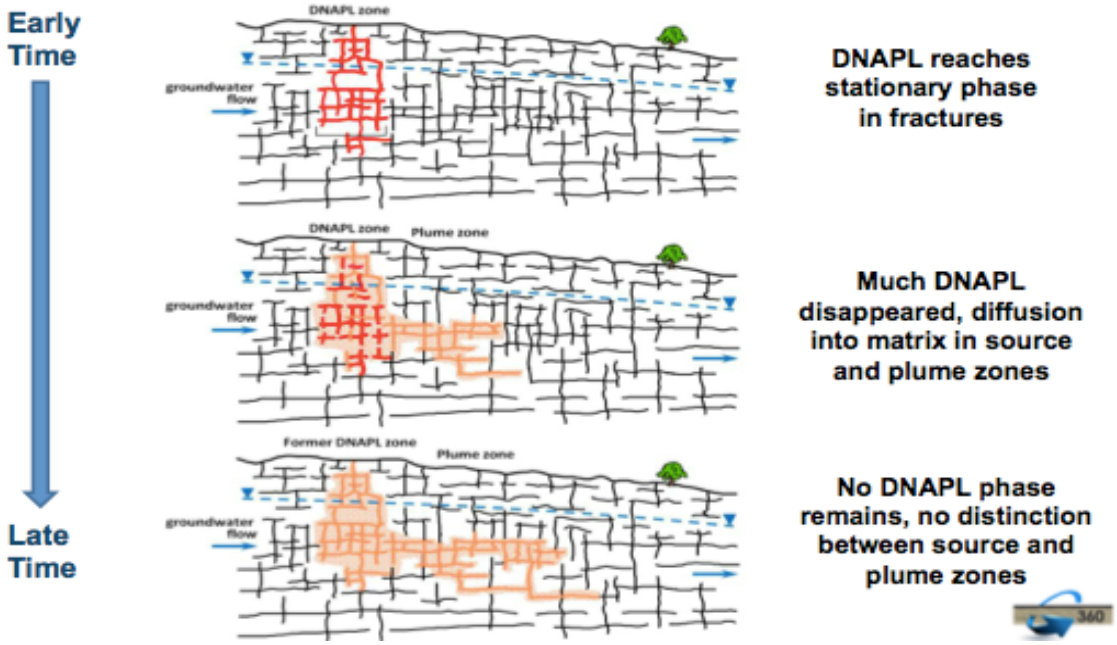

Figure 4 Evolution of Contaminant Source Zone and Plume in Sedimentary Rock (Cherry et al. 2009)

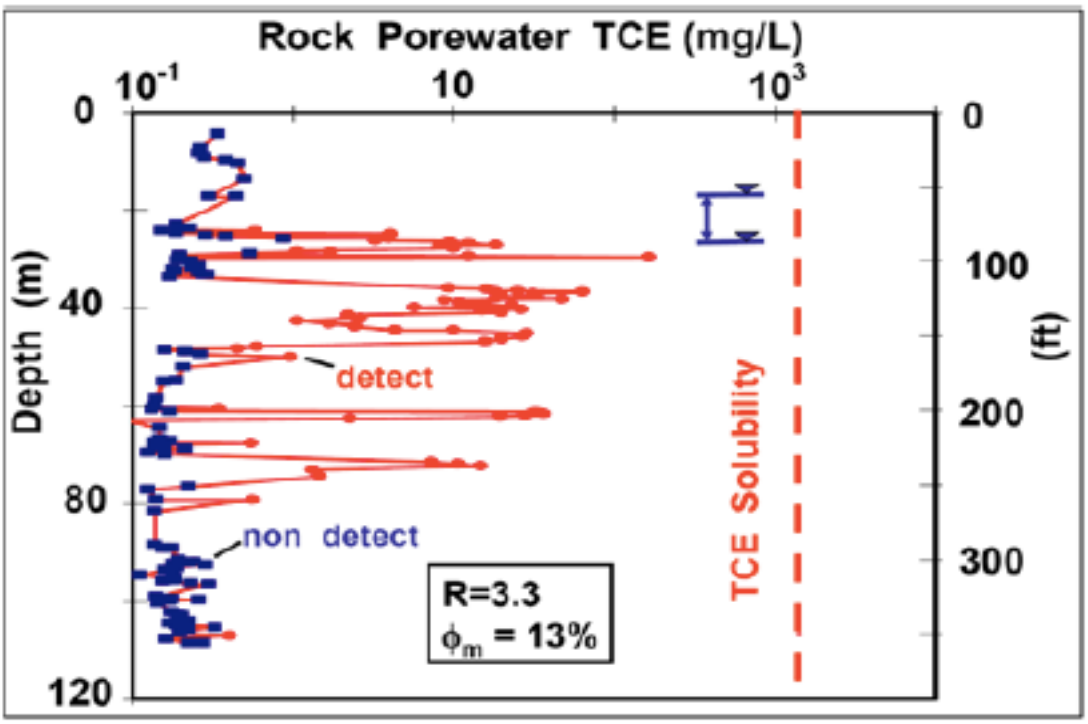

Figure 5 Measured Chlorinated Solvents in the Rock Matrix (Modified from Sterling et al., 2005)

1.3 Motivations and General Scope

There are several previous works on the site conceptual model that have been finished during the past decades of years. And they consider that the DNAPL penetrated to 100 m below the ground surface at this site. This hypothesis needs to be assessed using the CompFlow Bio model. As mention before, the DNAPL was emplaced starting in the late 1950's and the source zones are currently presumed to have dissolved into the ambient groundwater. This hypothesis will also be tested as part of the CompFlow Bio simulations. Based on results from the rock core VOC analysis, due to the contaminant mass storage is dominated by the rock matrix rather than the fractures. As early in 2012, McLaren et al suggested and utilized to model DNAPL plume emissions at the Smithvile site. And similarly in this study, the CompFlow Bio model will also be used to assess the different contribution of TCE aqueous phase mass flux emanating from the source zone via the matrix and discrete fractures. This mass flux is used as input into regional-scale groundwater transport models, and to reasonably determine downstream concentrations at points of regulatory interest. Finally, there is considerable uncertainty regarding the average aperture of the discrete fracture network. Estimates

values range from 75 mico meter to 150 micro meters depending on the method used assess the values. All of the above hypothesis will be tested over a range of the average fracture values.

Considering those three aspects listed above, we stated with 2D numerical model whose domain size is 50m x 0.3m x100m to find out how long it take for DNAPL in source zone to dissolve away; and then the rock core VOC analyses of the source zone and outflow boundary compared with field data from SSFL will be discussed. At last, mass flux of TCE in the aqueous phase exists the fence boundary in fracture and matrix was investigated. For represent more like the "real world", we applied these simulations on a 3D numerical model except that its domain size is restricted to be only 5m x 5m x15m because of computational limits.

A 2D simulation was conducted so that a domain that was 100m high could be simulated that was consistent with the onserved geology of the Santa Susana field site. Specifically, to capture the idea that TCE DNAPL had penetrated to a depth of 100m in a facture network with a spacing of 0.3m. As such, this resulting network was an extreme test of the current implementation of the CompFlow Bio model and a 3D representation of this geometry could not be constructed. Instead, a smaller 3D simulation using the same fracture geometry was constructed to assess any 3D effects on the TCE DNAPL distribution and subsequent dissolution. An additional constraint on the problem geometry was to neglect the vadose zone. This simplification was made to focus on the evolution of the TCE DNAPL beneath the watertable, to its final depth of 100m within the fracture network below the watertable. Simulating the emplacement of TCE within the vadose was the focus of Walton (PhD thesis ref), with this work serving as a continuation under the assumption that some TCE DNAPL has migrated thought he vadose zone and reached the watertable.

Physical processes such as dissolution, volatilization, sorption, diffusion and dispersion may occur concurrently with and be influential to the evolution of the source zone. These processes may lead to a plume of dissolved contaminant being transmitted away from the source zone over long periods via advective and diffusive fluxes of the solvent phase(s). Degradation processes may cause

the plume to become stationary or even recede. But sorption or decay isn't considered in this study and numerical dispersion is assumed to dominant physical dispersion, because dissolved transport is not of primary focus in this study (Walton, 2013).

Chapter 2

Methodology

2.1 General Conceptual Model

There are considerable literatures concerning karst fracture channel networks, for example, both Slough et al. 1999 and McLaren et al. 2012 use a 2D fracture rock domain with an intermediate fracture density at a spatial scale relevant to their NAPL source zone investigation on the Smithville site; the contaminants in sandstone fracture network system performing much different, especially the dissolution and diffusion transport can cause the residues of contaminant in porous rock matric as well as down-gradient fractures (Lipson et al. 2005). In both 1994 and 1997, Parker et al build up a conceptual model presenting the DNAPL performance in water-saturated fracture porous media. Sterling et al., 2005 and Pehme et al. 2007 use the rock core VOC method to investigate and conclude that both vertical and literal down-gradient migration of DNAPL with natural groundwater flow. And conceptual models with the VOC method also indicate that the diffusion occurs in both source zone and plume (Cherry, McWhorter et al., 2009).

With site and existing model data and the previous work of Walton, Unger and Parker (2010), a feasible conceptual model for a 3D inter-connected fracture network system including the spacing distribution, aperture, and length of fractures was built. The total system is in the saturated zone slightly below the water table, with only two phases (water and TCE) are involved as our hypothesis/ simulation effort.

In this conceptual model, 1% hydraulic gradient is chosen because the formal simulation models, such as Hurley et al., 2009 and Chapman et al., 2009, use the scenarios with a 1% hydraulic gradient after many previous field exploration tests on regional groundwater flow. And with the CompFlow Bio calibration, 1-phases flow (water) is firstly processed into a 2D vertical cross-section for model verification as well as adjust parameters for initial hydraulic conditions. And then, the DNAPL phase (TCE) is injected from the top of the domain into the system; and with around 10% of the precipitation (~46mm/year) (Walton, Unger et al. 2012), the infiltration dominants the vertical transport from the source zone. With this preparation, the conceptual model will be used for testing contaminant flow and transport behavior as well as plume migration, retardation and degradation.

2.2 General Numerical Model

Based on the overview provided by Narasimhan 1982 and Illman 2014, there are three main numerous approaches for conceptualizing flow and transport through fractured rocks: (1) Equivalent Porous Medium (EPM) models, which has inability to characterize the fracture and matrix in detail, and is inadequate in characterizing and/or monitoring groundwater movement and contaminant concentrations; (2) Continuum Models such as dual-porosity (DP) or dual-permeability (DK), which may not be uniquely defined for a given geological setting due to the use of a shape factor scaling the mass transfer between the matrix and fracture continua (Unger, 2004), and this class of model is hard to handle fracture cross flow and two-phase context transfer function because fractures do not cross-cut the matrix (Hoteit, 2008); (3) Discrete Fracture Network Models (DFNM), which provide high-resolution predictions of groundwater flow and contaminant transport because fractures are explicitly considered. And DFN models incorporating three mobile phases have been used in petroleum reservoir problems (Walton, 2013).

Slough et al., 1999 used the numerical model CompFlow to study the effects of grid discretization on the migration of DNAPL within a discrete-fracture network embedded in a porous rock matrix; their simulations compared different methods of grid discretization, and highlight the importance of grid refinement when simulating DNAPL migration problems in fractured porous media. Following directly from Slough et al., Walton, 2013 derived how small volume CVs, which arise at the intersection of fractures in three dimensions, may be algebraically eliminated from the numerical system. In 2004, Reynolds and Kueper used the multiphase compositional numerical model QUMPFS to investigate the migration of Dense, Non-Aqueous Phase Liquid (DNAPL) and dissolved phase contamination through a fractured heterogeneous porous medium. And Walton, 2013 used similar approaches of Reynolds and Kueper, such as no distinction is made between the hydraulic aperture and the mechanical aperture of a fracture and the effect of fracture roughness is captured by macro-scale relative permeability and capillary pressure relationships.

For simulation of DNAPL in this task, we employ the numerical model CompFlow Bio. This numerical model simulates isothermal flow and transport of three components (water, air and an oil/contaminant species) in three mobile and mutually interactive phases (aqueous, gas, and nonaqueous) in a 3D porous medium (PM) and discrete fracture network (DFN) domain using a first-order accurate, finite-volume formulation (Walton, 2013). Figure 6 presents the novel aspects: 1) direct PM-to-PM flow across a fracture plane via asperity contact bridged flow; 2) PM control

volume (CV) bisection to insert axis aligned, orthogonal, rough-walled fractures resulting in an unstructured mesh; and 3) algebraic reformulation of the flow equations to remove small CVs at the intersection of three fractures (Walton, 2013). In this case, the simulations focus on two-phase, nonaqueous (TCE) and water, in heterogeneous media referred to the discrete fracture network in porous medium.

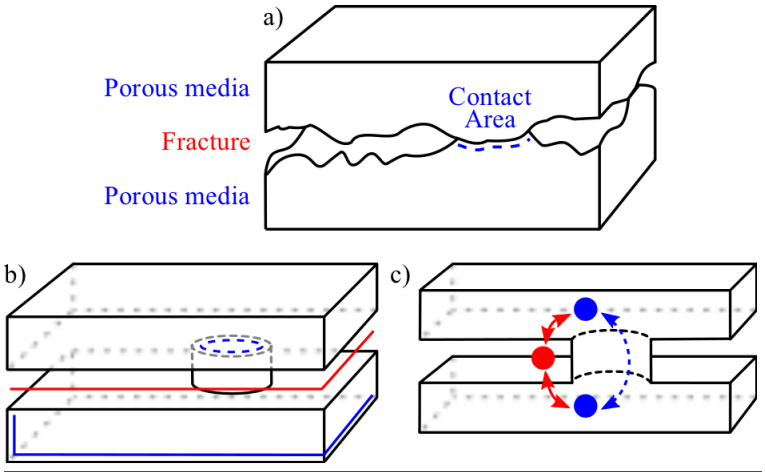

Figure 6 Discrete fracture conceptualization showing a) a schematic of a rough-walled fracture, b) the two dimensions of a planar fracture CV (red lines), three dimensions of a matrix CV (blue lines) and some asperity contact area (blue dashed line), and c) connection between adjacent PM blocks via asperity contact area (blue dashed arrow) and the contact of PM with the fracture CV (red arrow). (Walton, 2013)

2.3 The rock CORE^{TM} VOC method and Virtual Core Sampling

The spatial distribution of contaminants within chlorinated solvent plumes in fractured sedimentary rock exhibits strong variability due to heterogeneity in source zone contaminant mass distributions, fracture network and matrix characteristics accompanied by temporal variability in groundwater flow. Therefore, one major reason why so little is known about contaminant migration and fate in fractured sedimentary rock is that traditional research approaches involve only sampling water from the fractures. However, field studies using the rock core VOC analysis method show that contaminant mass storage is dominated by the rock matrix rather than the fractures, and the contaminant concentrations in the fractures and the matrix are not in equilibrium (Hurley and Parker, 2002; Sterling et al., 2005). Figure 7 illustrates use of rock core contaminant analyses to identify migration pathways by identification of diffusion haloes associated with active fractures.

In 1997, B.L. Parker and colleagues developed a method for determination of VOC concentrations in rock core that involved crushing the core samples with extraction in methanol over several weeks. Through collaboration with T. Górecki, the method evolved to rapid microwave extraction and very low detection limits. The advanced suite of procedures, referred to as the CORE™ (Characterization of Rock Environments) approach for discrete fracture network (DFN) investigations, include methods for sampling, extracting and analyzing contaminants present within the rock matrix to assess the effects of diffusion of contaminants from fractures into the rock matrix (Figure 8).

With rock core VOC analysis data sent from SSFL, we use the virtual core sampling method (Walton, unpublished, 2013) to present concentration distribution of different phases (NAPL and dissolved) of TCE in both matrix and fracture with depth (Figure 9).

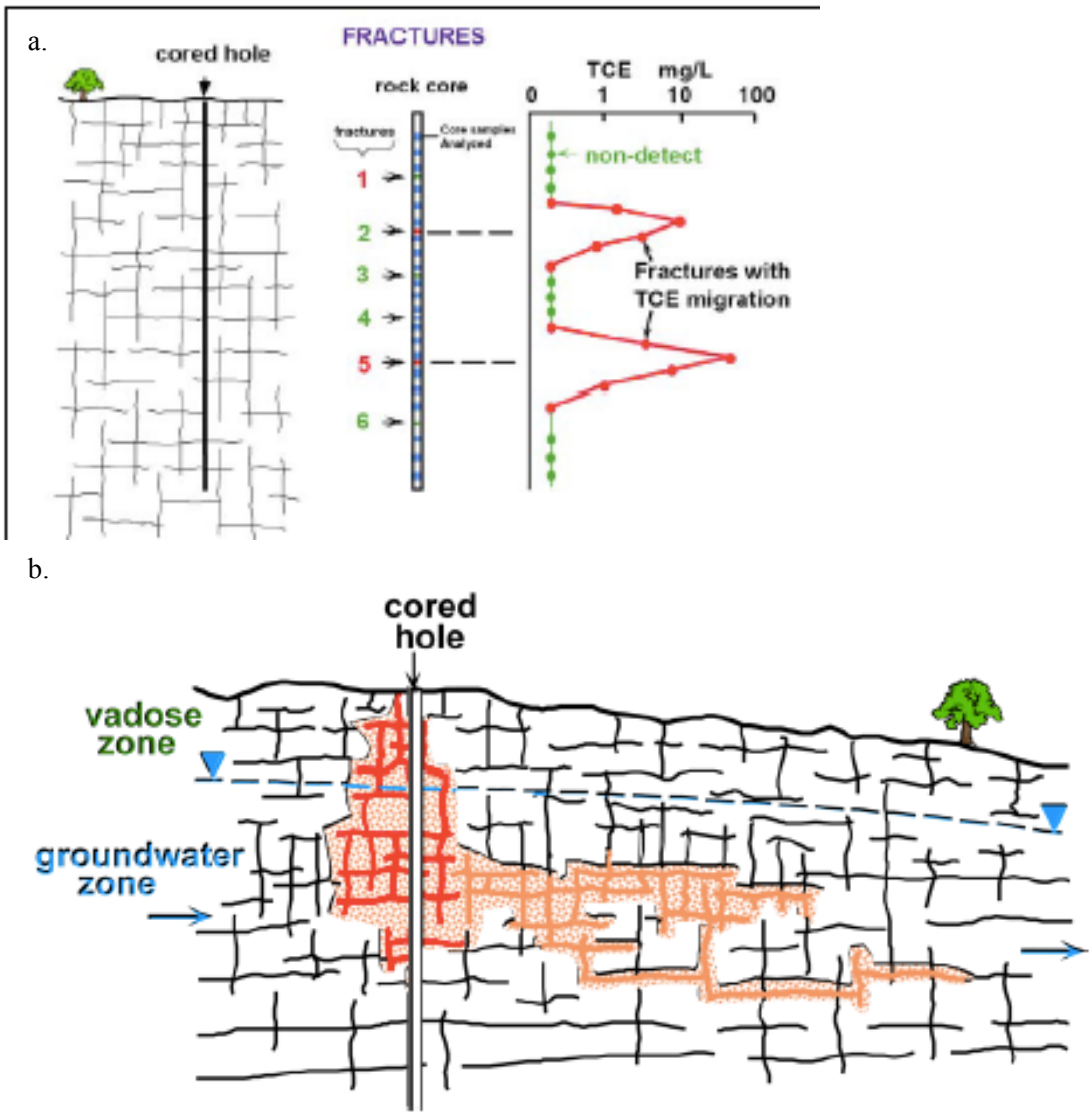

Figure 7 a. Typical sampling distribution. Very close sample spacing is necessary to determine mass distribution and pathways. b. Cored hole in contamination source zone. (Parker & Sterling, 2009)

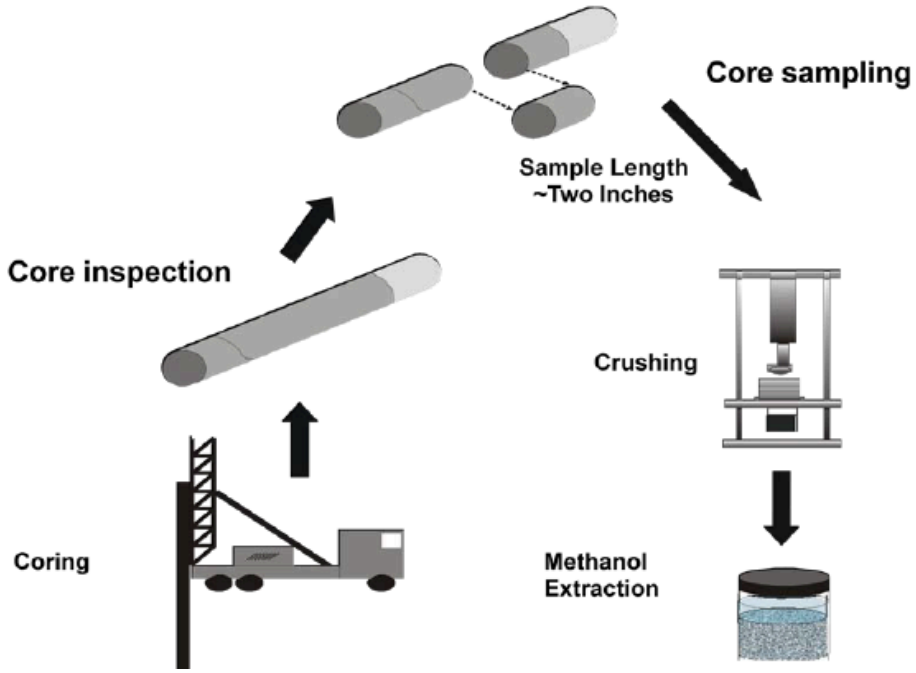

Figure 8 Rock CORE VOC method (Parker & Sterling 2009)

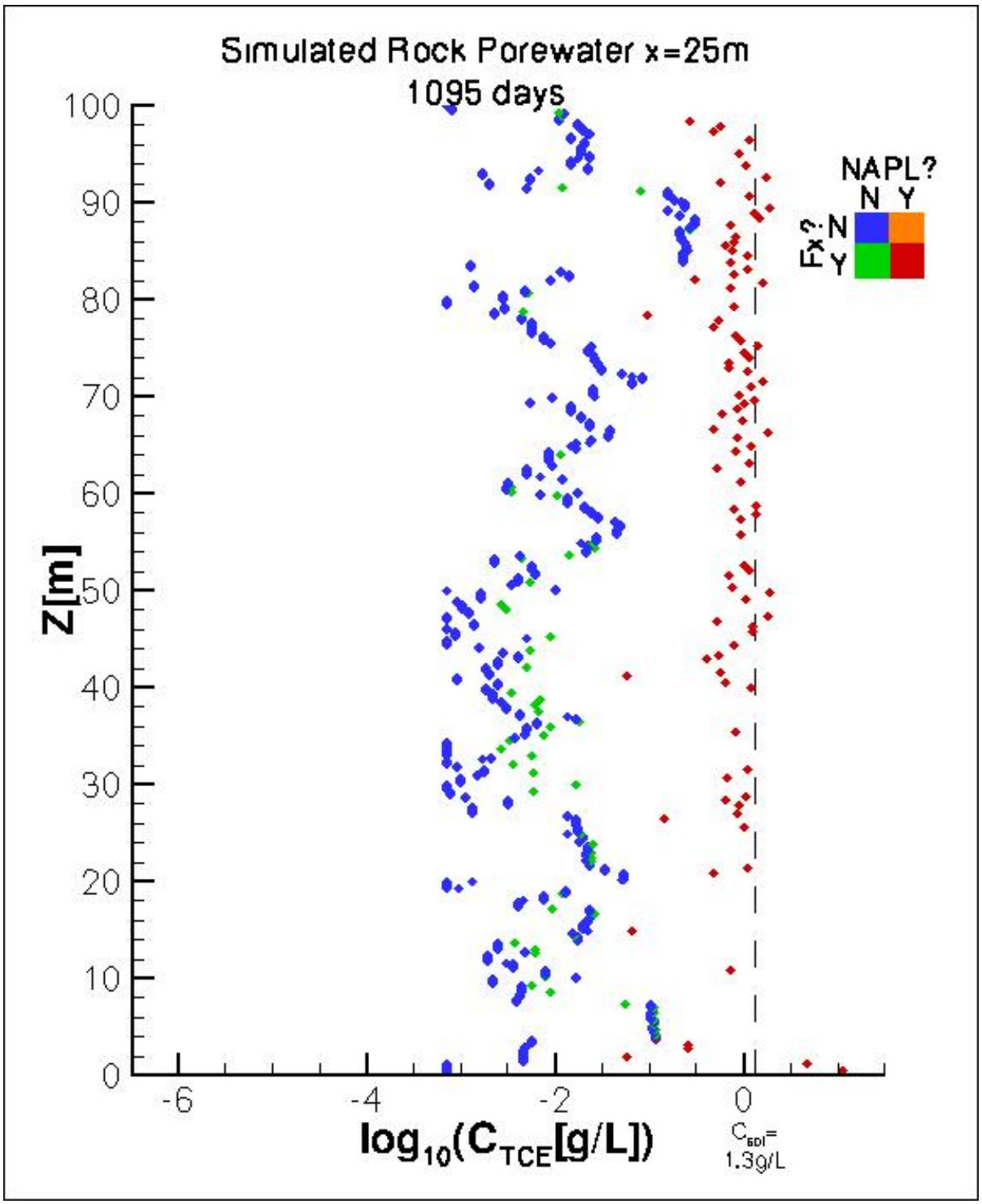

Figure 9 An example of the virtual core sampling method

The main idea of virtual core sampling method firstly parses the node input file and finds all PM and Fracture control volumes that are intersected by the vertical line (i.e. the "virtual core hole") through the area with 0.15m radius around the location of virtual in the domain (Figure 10); and then parses the output file of the numerical model and performs calculations to determine the mass and concentration of TCE in cylindrical rock core samples.

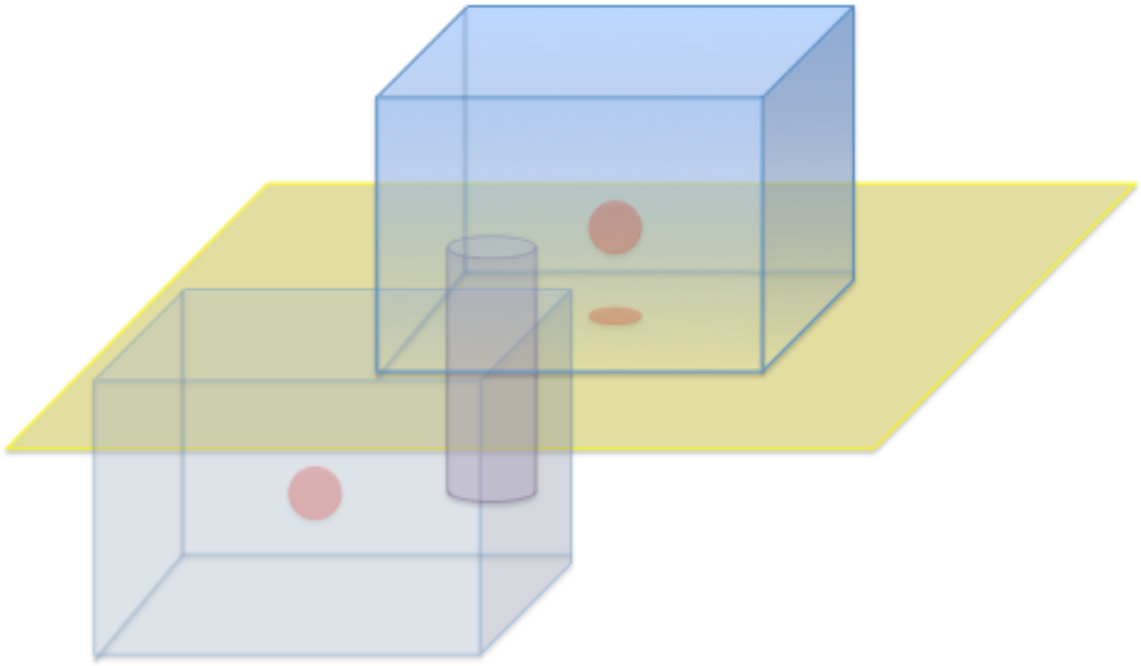

Figure 10 Conceptual diagram of a virtual core (purple cylinder) intersects two nodes (blue box). The yellow plane presents the intersected plane between two nodes, and red spots present the center of each node.

Calculations in the virtual core sampling method (Walton, unpublished, 2013):

Calculation of the Total Moles of TCE

a) In NAPL phase

$$\sum_{\forall_i} S_{n,i} \cdot \left(V_i \cap V_{cyl}\right) \cdot {M^*}_{TCE} \cdot \emptyset_i$$

$S_{n,i}$: Saturation of NAPL-phase TCE in node i [-]

V_i : Volume of node i [L]

V_{cyl} : Volume of the cylinder [L]

${M^*}_{TCE}$: Moles of NAPL-phase TCE [-]

$*$: Exclude vertical fractures

$\emptyset_i$: Porosity of node i [-]

b) In aqueous phase

$$\sum_{\forall_i} S_{q,i} \cdot \left(V_i \cap V_{cyl}\right) \cdot M_{q,i} \cdot X_{TCE,q} \cdot \emptyset_i$$

$$M_{q,i} = [\,1 + \widehat{C_q}\left(P_i - P_{ref}\right)] \frac{{M^*}_{TCE}\, {M^*}_w}{{M^*}_{TCE} X_{w,q} + {M^*}_w X_{TCE,q}}$$

$S_{q,i}$: Saturation of aqueous-phase TCE in node i [-]

$M_{q,i}$: Moles of aqueous-phase (water and TCE) in node i [-]

$X_{TCE,q}$: The proportion of TCE in aqueous phase [-]

$\widehat{C_q}$: Compressibility of the aqueous phase [1/kPa]

P_i : Pressure of node i [pa]

P_{ref}: Pressure of reference node [pa]

M^*_w : Moles of water [-]

$X_{w,q}$: The proportion of water in aqueous phase [-]

Calculation of the total volume in pore space

$$V_{pore} = \sum_{\forall_i} (V_i \cap V_{cyl}) \cdot \emptyset_i$$

V_{pore} : Total volume in pore space [L]

Calculation of the blended concentration of TCE (Assume all water in pore space)

$$C_{TCE,q} = \frac{(M_{a)} + M_{b)}) \cdot W_{TCE}}{V_{pore}}$$

$C_{TCE,q}$: Blended concentration of TCE [mg/L]

$M_{a)}$:Total moles of NAPL-phase TCE [-]

$M_{b)}$:Total moles of aqueous-phase TCE [-]

W_{TCE} : Molar weight of TCE [mg/mole]

Chapter 3
Parameters

3.1 Parameters to build the grid

The fracture network of our conceptual model is widely distributed in the Chatsworth Formation. The rock matrix porosity and permeability for the Chatsworth Formation has been rigorously determined by laboratory measurements using several methods including both conventional and advanced microscopic imaging methods. All lines of evidence indicate that the rock matrix porosity is relatively large nearly everywhere. This supports the major conclusion of the SCM that the rock matrix is strongly conducive to diffusion driven chemical mass transfer between the fractures and the rock matrix, providing a large storage reservoir for all types of contaminants. Figure 11 presents the distribution of the matrix porosity (ϕm) within the Chatsworth Formation. The porosity is ranges from 3% to 20% with a geometric mean value of 13.6% for SSFL sandstone (data from Hurley, 2003). Thus, the porosity of our conceptual model is set to be 0.13. Absolute permeability values for fractures are calculated using the effective hydraulic aperture in the cubic law as discussed in Walton's thesis, 2013. The rock matrix simplified to be a homogeneous porous medium based on the C4-137 sample of Amirtharaj et al., 2011; its permeability is set to km = 1.0×10^{-15} m^2.

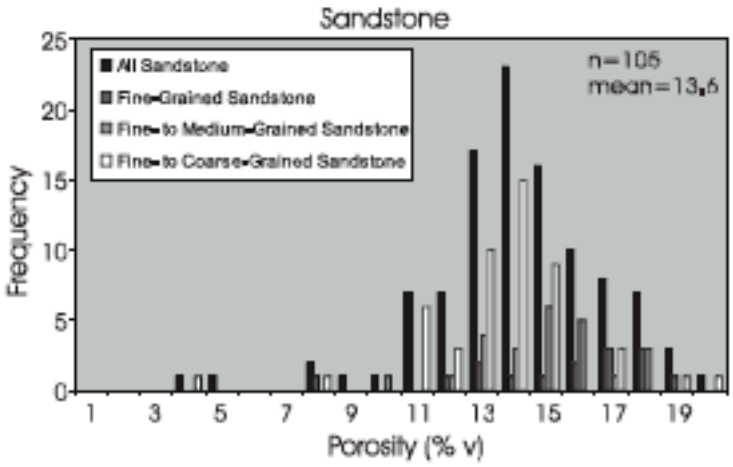

Figure 11 The distribution of the matrix porosity (ϕm) within the Chatsworth Formation (Hurley, 2003)

Achieved from the drill cores analysis, Cherry, McWhorter et al. 2009 found that the length of fractures is small to moderate with a range from 0.5 to 20m at site; with statistic data analysis, they

presents the variable apertures on a log-normal distribution and variable length in both vertical direction and horizontal direction (Figure 12). The most proportion in both directions is 125 microns. In addition, 50~175 also get larger proportions of fracture apertures. Therefore, our original purpose is to use 75, 100, 125, 150 microns 2b values in both 2D and 3D conceptual model so as to determine the most reasonable 2b value for DNAPL simulation. But only 75 and 100 microns 2b value used in the 2D simulation due to computational limits, though all the microns 2b values used in the 3D simulation with smaller domain size. The fracture density is calculated from fractures hit by arbitrarily placed scan lines (three to seven in each axial direction), analogous to counting fractures that intersect a borehole drilled in rock (Walton, 2013); and the fracture density in our conceptual model is set as an average 3 fractures per meter. In addition, the fractures are random distributed and connected but maintain the orthogonal relationship in vertical (x-z) and horizontal (z-y) directions. Table 1 summarizes the key simulation parameters to build the domain grid.

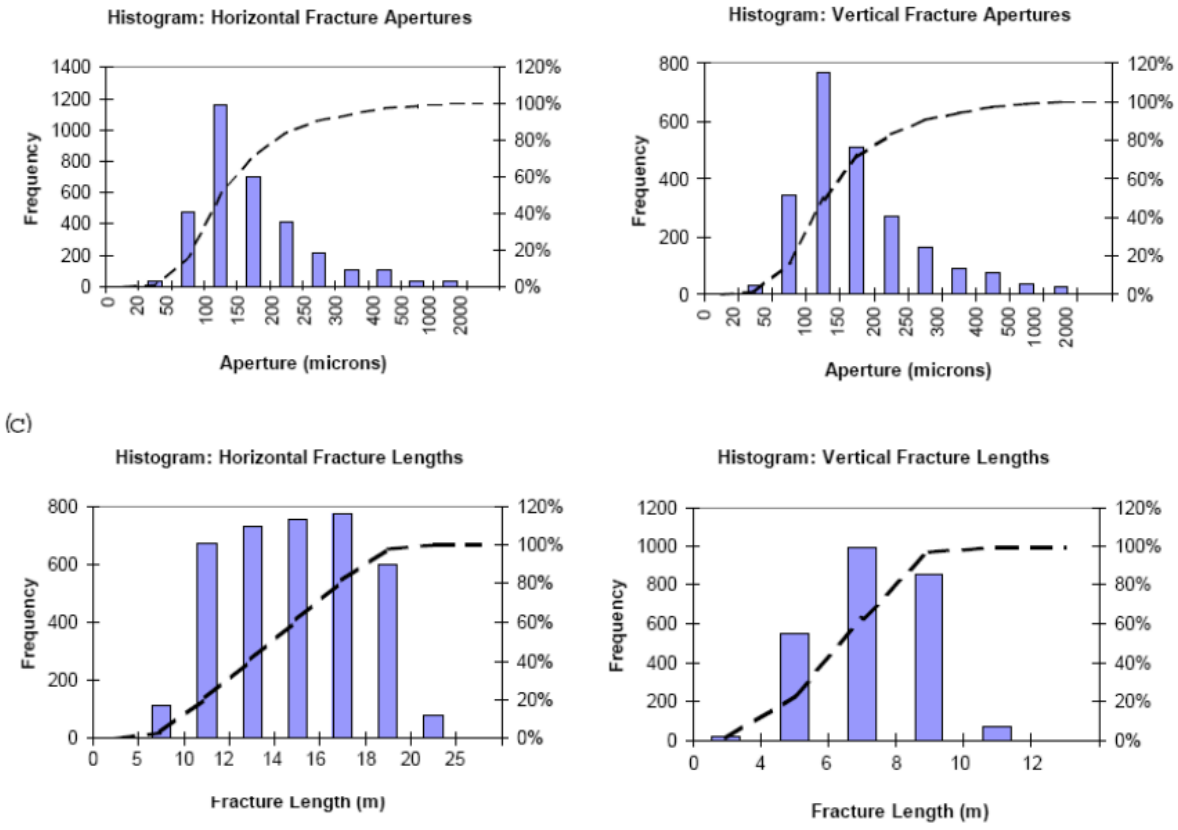

Figure 12 Frequency of variable apertures on a log-normal distribution, and variable length (Cherry, 2009)

Table 1 The key simulation parameters to build the domain grid

Parameters	Value	Unit
Matrix permeability, k_m	1.0×10^{-15}	m^2
Matrix porosity, ϕ	0.13	-
Fracture density	≈3	m^{-1}
Fracture aperture, 2b	75~150	μm

Relative permeability and capillary pressure relationships are read in to the model from tabular data (see for example Tables 2 and 3 in Freitas et al., 2009). The benefit to tabular inputs is that they allow the underlying kr-S or Pc-S functional relationships to be substituted at will, without modification to the model's source code. However, attention must be given when interpolating between the discrete data points in the tables. (Walton, 2013)

3.2 Parameters to run the simulation

In this conceptual model, 1% hydraulic gradient is chosen since the regional-scale groundwater simulation models indicate a 1% hydraulic gradient after many previous filed exploration tests on regional groundwater flow. And the infiltration rate is set based on the average annual precipitation rate of 18 in/year (Walton's thesis, 2013). We select the rate of injection in the 2D conceptual model as ~2 L/d, i.e. one "55 gallon drum" of TCE per month; but the rate of injection in the 3D model as ~0.6L/d in the 3D conceptual model due to computational limits. Table 2 summarizes the key simulation parameters to run the simulation.

Table 2 The key simulation parameters to run the simulation

Parameters	Value	Unit
Hydraulic gradient	0.01	-
Recharge	18	in/year
Injection Rate (2D)	2	L/d
Injection Rate (3D)	0.6	L/d

Chapter 4

Two Dimensional Numerical Model

4.1 Domain description

Base on conceptual model domain, we have built numerical models focused on the TCE flow and transport habit under groundwater flow conditions. We started with a 2D domain with 50m x 0.3m x 100m in x-, y- and z- directions, to simulate two- phase fluid (water and TCE) in medium. Therefore, the domain is set several meters below the water table (saturated without air phase). The simulation domain is shown on Figure 13. The fractures feature in this simulation is basely maintain the features tested from the sample at the SSFL. In this 2D domain, the fractures are only distributed in xz- and xy- directions, and there are about 5000 fractures in total. The aperture of fractures in the domain is set to be 75um and the density of fractures is set as approximate 3 per meter. In the domain, the permeability of fracture is about $5x10^{-10}m^2$, and the permeability of matrix is about $1x10^{-15}m^2$.

Both recharge and TCE load are applied at the top of the domain, with setting the permeability and porosity of porous media at the top greater than the rock matrix to permit down flow direction, TCE primarily dominate the vertical flow path. The TCE was injected within a single horizontal fracture of dimension 4mx1m in order for the resulting TCE DNAPL to collect and migrate within the fracture network instead of the matrix. The horizontal fracture provides various entry points for the injected TCE to naturally flow into the fracture network. Beneath the watertable, TCE DNAPL will preferentially reside within the fractures given the large entry pressure for oil to enter the matrix. Furthermore, the fractures have a much greater permeability than the matrix, facilitating the injection and subsequent migration of the TCE DNAPL source zone.

Another important condition is the lateral groundwater flow (Figure 14). To maintain a constant pressure conditions for natural groundwater flow, two thin fractures (red and blue planes) are settled on both left and right side. On the left side, an injection well injects water into the fracture at the bottom of the fractures; on the other side, a pumping well is set at the bottom of the fracture. The combination of the two wells can force a lateral groundwater condition with constant pressure, which is called steady state. The combination of vertical inflow and outflow factures permit a single source sink term connected to each fracture to control lateral flow across the domain in a natural manner. More specifically, the large contrast in permeability between the heterogeneous fracture aperture

distribution and the background matrix make it impossible to control horizontal flow across the domain by specifying a constant head condition and the inflow and outflow boundaries. Instead, by letting these vertically continuous fractures naturally connect to the fracture network, injected water can then distribute itself across the inflow boundary and proceed horizontally across the domain towards the outflow fracture, where it is then collected and funneled towards the single sink term.

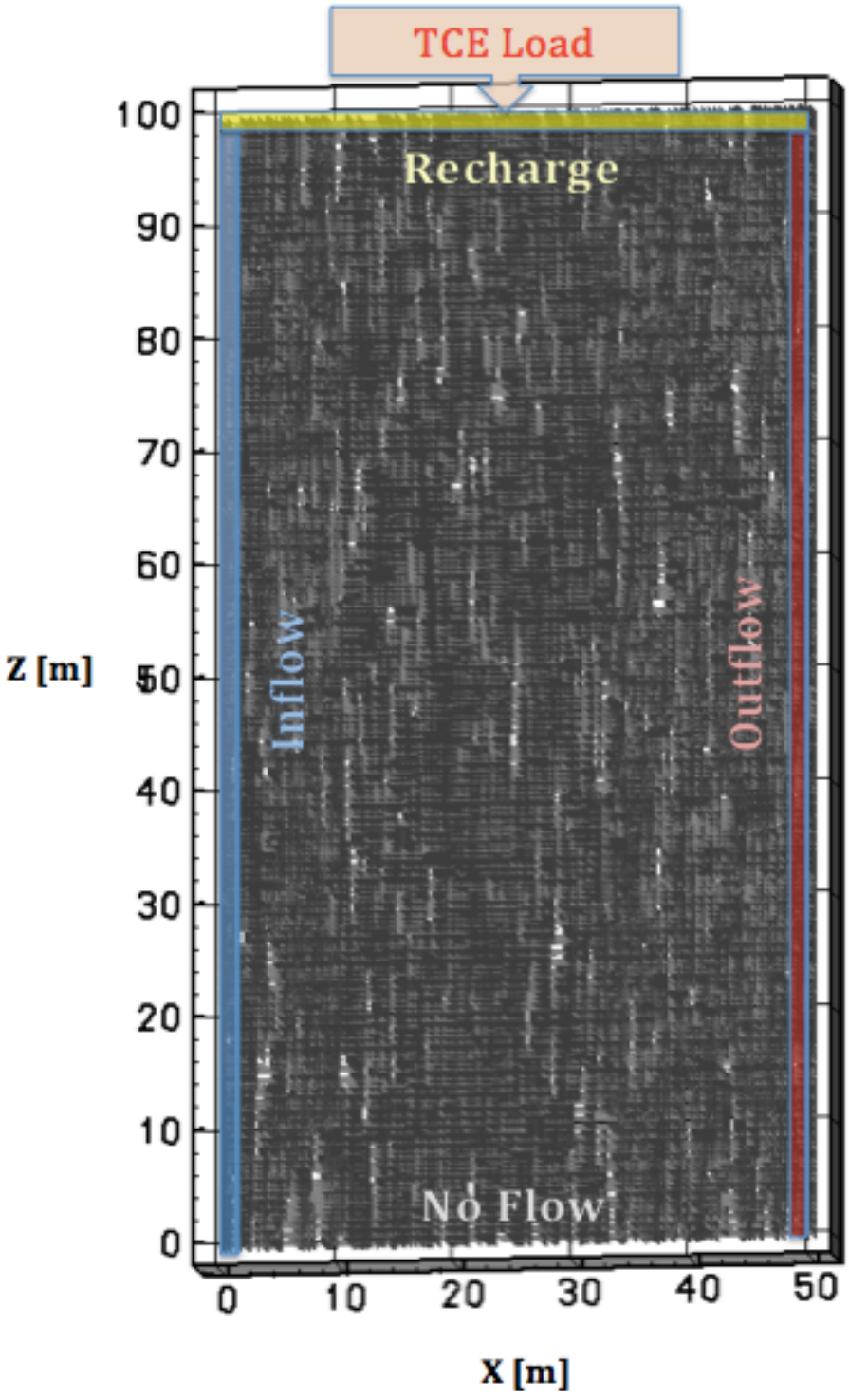

Figure 13 Boundary condition setting in the 50mx0.3mx100m domain conceptual model.

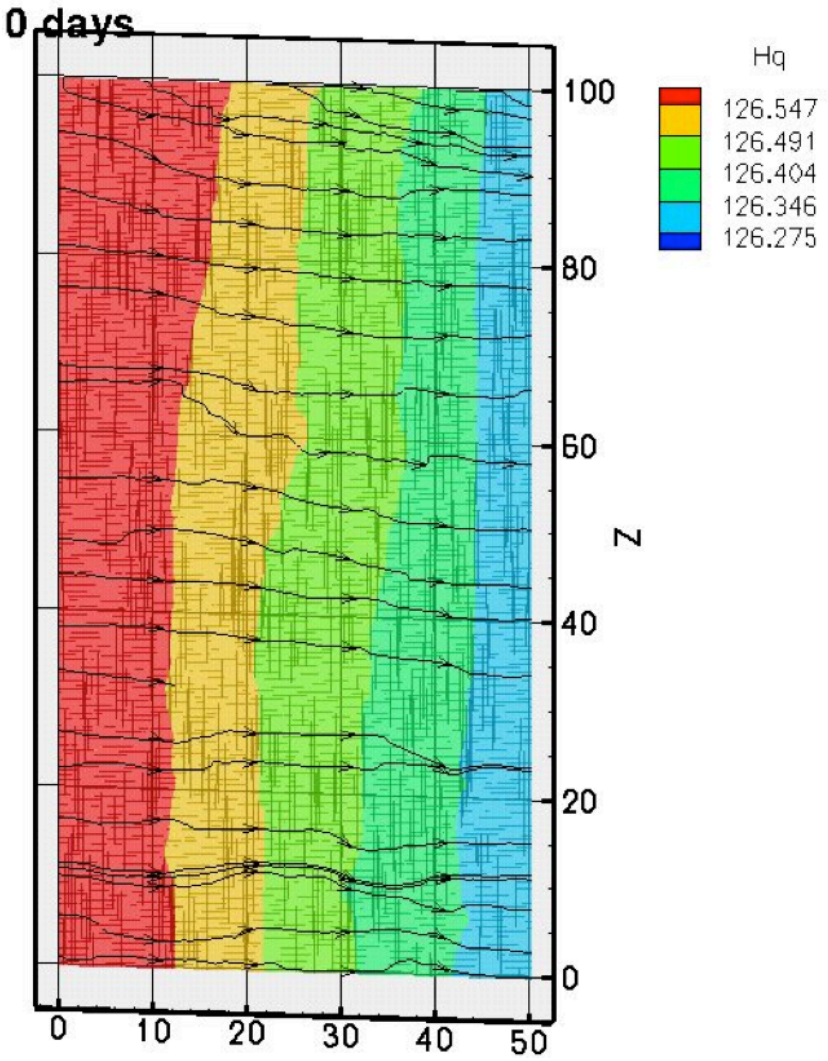

Figure 14 Hydraulic head contours

However, the injection rate of the injection well is required to be carefully determined to maintain the 1% hydraulic gradient for 2D TCE infiltrate simulation. An example of the wells setting in this case by CompFlow is shown in Figure 15. Well 1 is the injection well on the top of the domain to form recharge event (0.0019 m3/day). Well 3 in the injection well on the left boundary injects water at a constant rate of 0.00015 m3/day, while the pumping well 4 is set on the right side with a constant pumping rate at 0.0025 m3/day. Within the allowance error, it never gets to a "perfect" steady sate; and with the 0.4L/d (0.0004m3/d) difference allowance, this combination of an injection well and a pumping rate forces the later water flow under constant pressure head gradient.

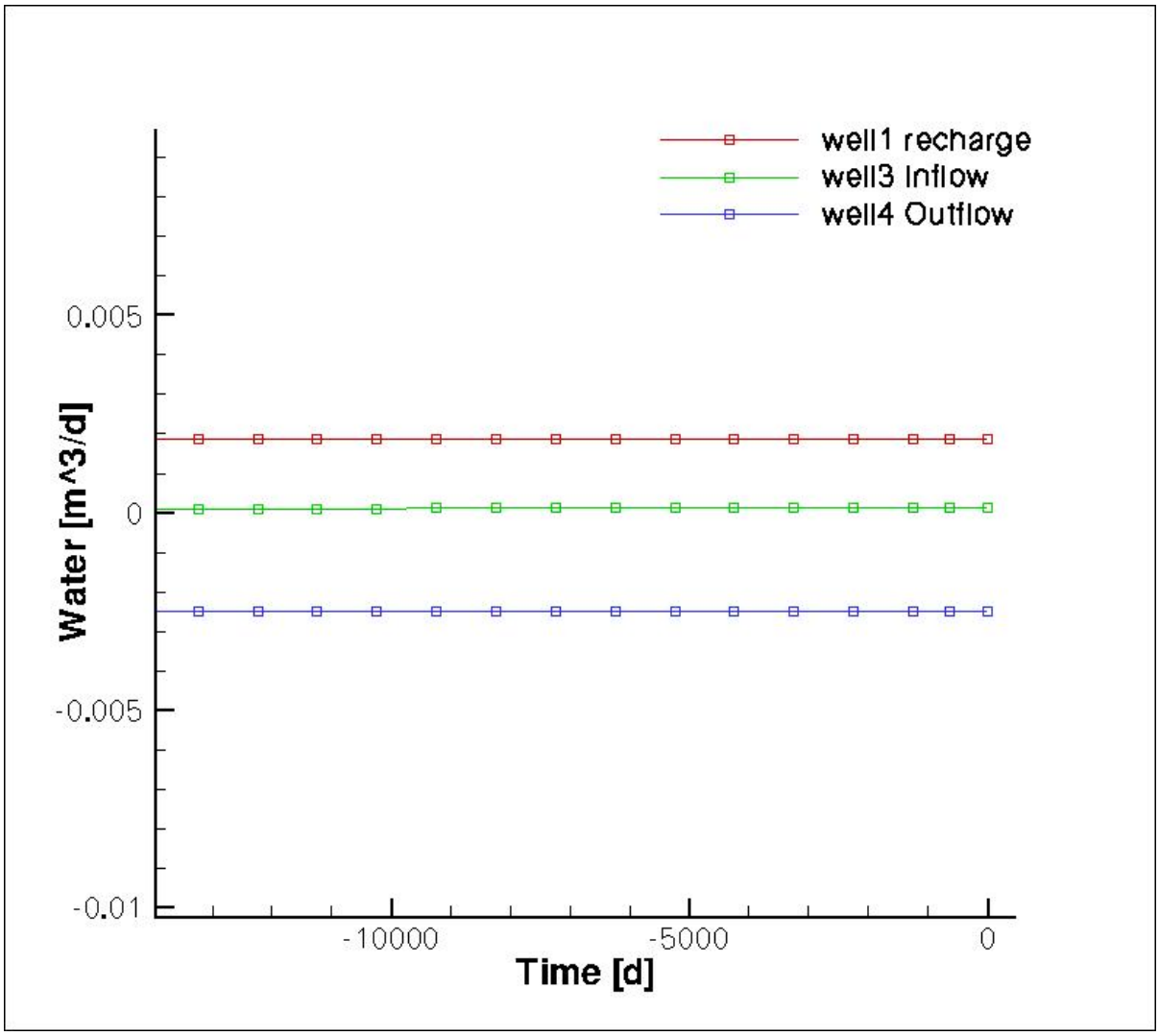

Figure 15 Water injection/pumping versus time, an example to illustrate how the wells settle the boundary conditions

The bulk hydraulic conductivity can be estimated with Darcy's Law once the domain reach the steady state, and the bulk hydraulic conductivity with different apertures in 2D simulations are shown in Table 3.

$$K_{bulk} = \frac{Q}{A \times i} = \frac{0.00249\, m^3/day}{(100m \times 0.3m) \times (0.01)}$$

$$= 0.0083 m/day \; = 0.961 \times 10^{-7} m/s$$

K_{bulk} ： The bulk hydraulic conductivity [m/s]

Q ：Flow rate [m^3/day]

A ：The area where the fluid flow through [m^2]

i ：Hydraulic gradient [-]

Table 3 The bulk hydraulic conductivity with different apertures in 2D simulations

2b [um]	Q[m^3/ day]	K_{bulk}[m/s]
75	0.00249	9.60E-08
100	0.00399	1.54E-07

4.2 Water/DNAPL simulation results in 2D domain

In this 2D domain, the TCE is injected at 2 L/day in a small horizontal area on the top center of this domain, which just below the boundary layer, and below the water table. TCE is not expected to bind with soil particles or bioaccumulate. Since it is heavier than water and has a low solubility value, TCE is classified as a dense nonaqueous phase liquid, or DNAPL. This class of chemicals will tend to sink through the water column (both surface and ground) until they encounter a barrier that is sufficiently impermeable to stop them (Howard &Publishers, 1991). After about 4 simulation days running (Figure 16), the NAPL of TCE reached the impermeable bottom boundary of the domain with fracture aperture sizes 75~150μm. Generally speaking, the infiltration flow dominants the TCE migration in saturated zone, and mainly in fracture network. The infiltration speed in vertical direction is very fast, approximate 25m/day. The fast infiltration flow in fractures is likely due to the well-interconnected fracture system, very dense fracture distribution (3 fractures/meters), and extremely low matrix permeability. And due to fast infiltration flow in fractures, Little lateral migration of TCE is detected.

Lateral advection of the aqueous phase TCE plume under the natural groundwater floor condition is obvious with an approximate speed of 1m/day. The diffusion and dispersion transport is found in both matrix and fractures and in both vertical and horizontal directions. Figure 17 shows that the evolution TCE DNAPL distribution within the fracture network show very little horizontal spreading, and is instead focused into a narrow column extending vertically downwards from the injection point to the base of the domain. This is a consequence of very close spacing of the factures of approximately 0.3m effectively permitting a continuously connected high-permeability pathway of fractures to channel the flow downwards. Strong horizontal spreading was observed in previous simulations when the fracture spacing was increasing to 1 fracture every 10m. This sparse fracture network required large lateral deviations in the migration of the TCE DNAPL source zone in order to find a continuously connected high-permeability pathway downward though the domain.

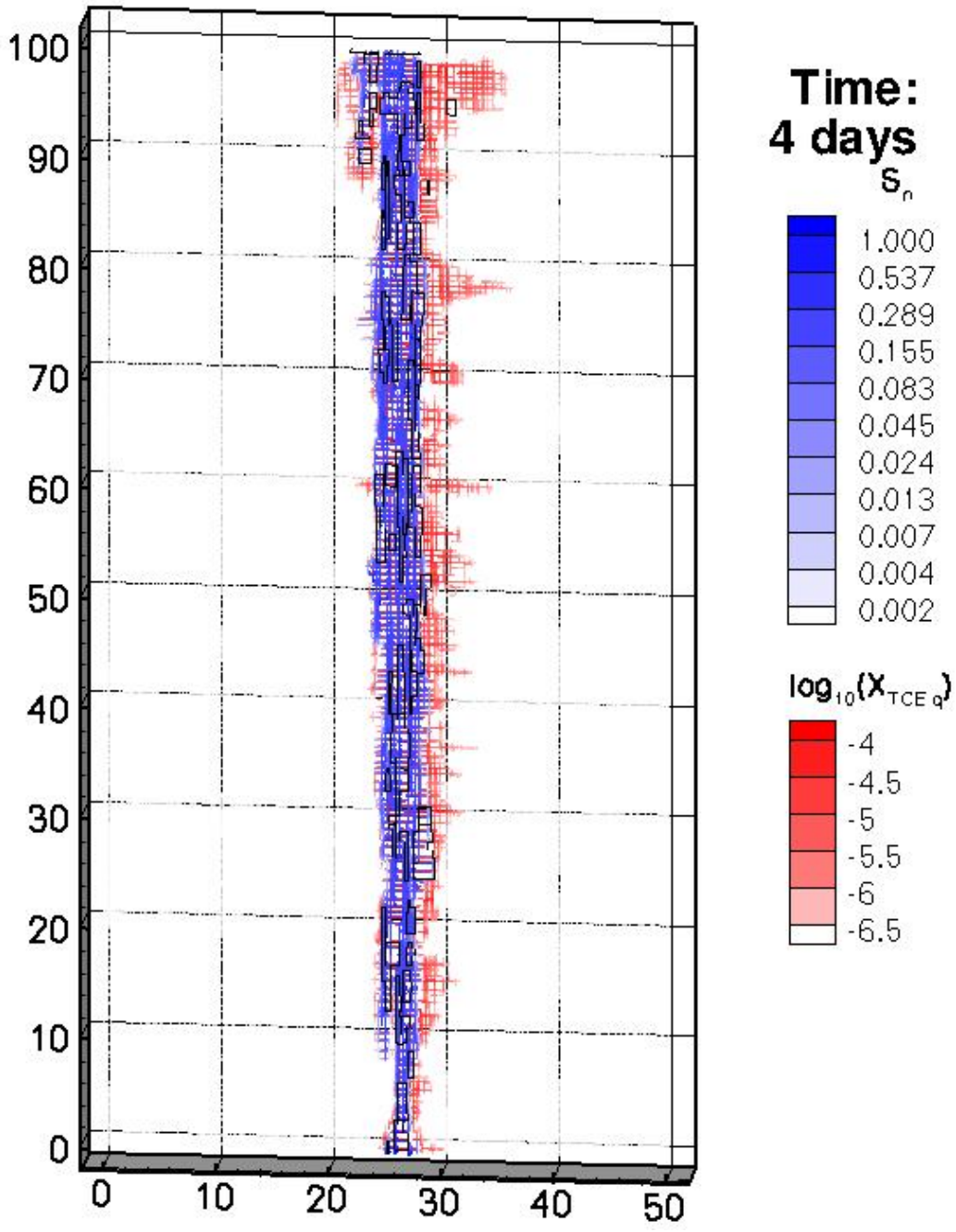

Figure 16 DNAPL and Plume Architecture of 2b=75μm case (100m penetration in 4 days)

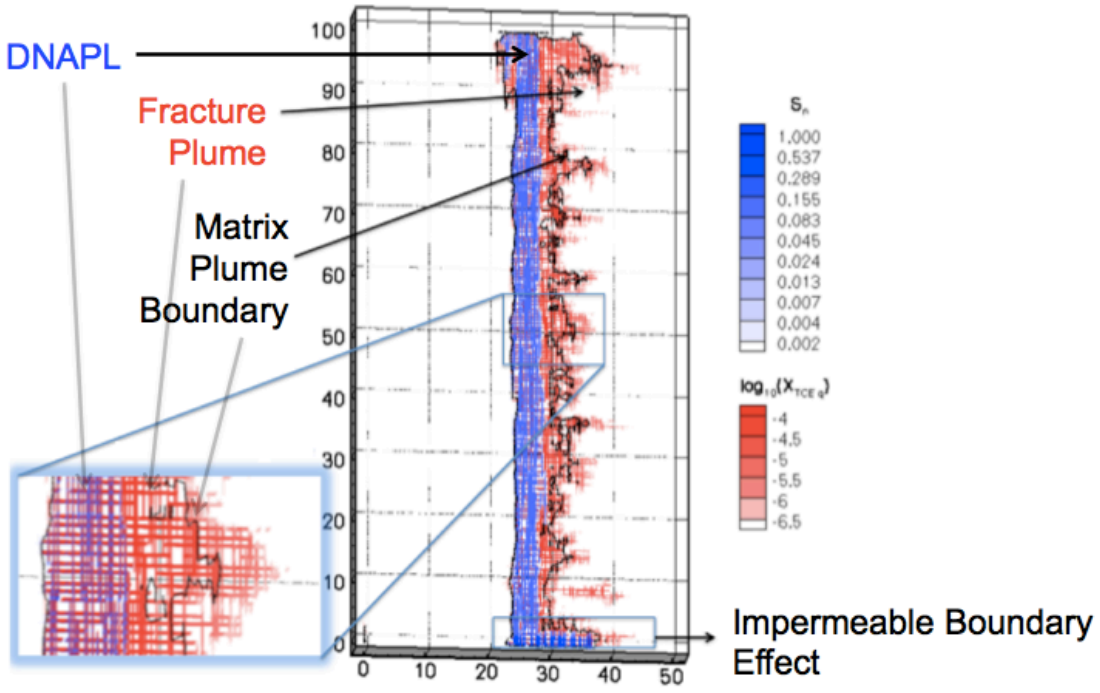

Figure 17 TCE contour plot of 2b=75μm case (dissolved plumes in both matrix and fractures, and lateral advection and dispersion)

4.3 The rock CORE™ VOC method

In the 2D simulation, to assess the effects of diffusion of contaminants from fractures into the rock matrix, 2 virtual cores (core A and B) are set to vertically penetrate through the domain (Figure 18). Core A is set though the middle axle of the domain at about x=25m, and core B is set though the outflow boundary of the domain at about x=49m.

Base on the sample data collected at SSFL via the rock CORE™ VOC method, an example of the distribution of TCE concentration among fracture and matrix at both location of the domain are present on Figure 19 and 20. In soils TCE often will leave a residual in pore spaces where the capillary pressure is strong enough to keep them from flowing. Once stopped, they and any residual will become a dissolved phase source for a very long time (Howard &Publishers, 1991). There are four cases for TCE to distribute in the domain: TCE appears as NAPL in both matrix (orange dot) and fracture (red dot), meanwhile, TCE dissolve in water and present in both matrix (blue dot) and fracture (green dot).

After about 8 simulation years running, some features can be summarized. TCE as NAPL phase is mainly restrict through the middle axel of the domain where x=25m, but hardly detect near the outflow boundary at x=49m; the concentration of NAPL is very close to the solubility of TCE, which is about 1.3g/L. It's hard to tell any relations between the concentration of dissolved phase of TCE with depth near the middle axel of the domain, and the concentration of TCE fluctuates between 0.001g/L to 1.3g/L. But near the outflow boundary, TCE starts to disappear from the top of the domain to about 15m deep; moreover, the range of TCE concentrations decrease to 0.01g/L to 0.1g/L.

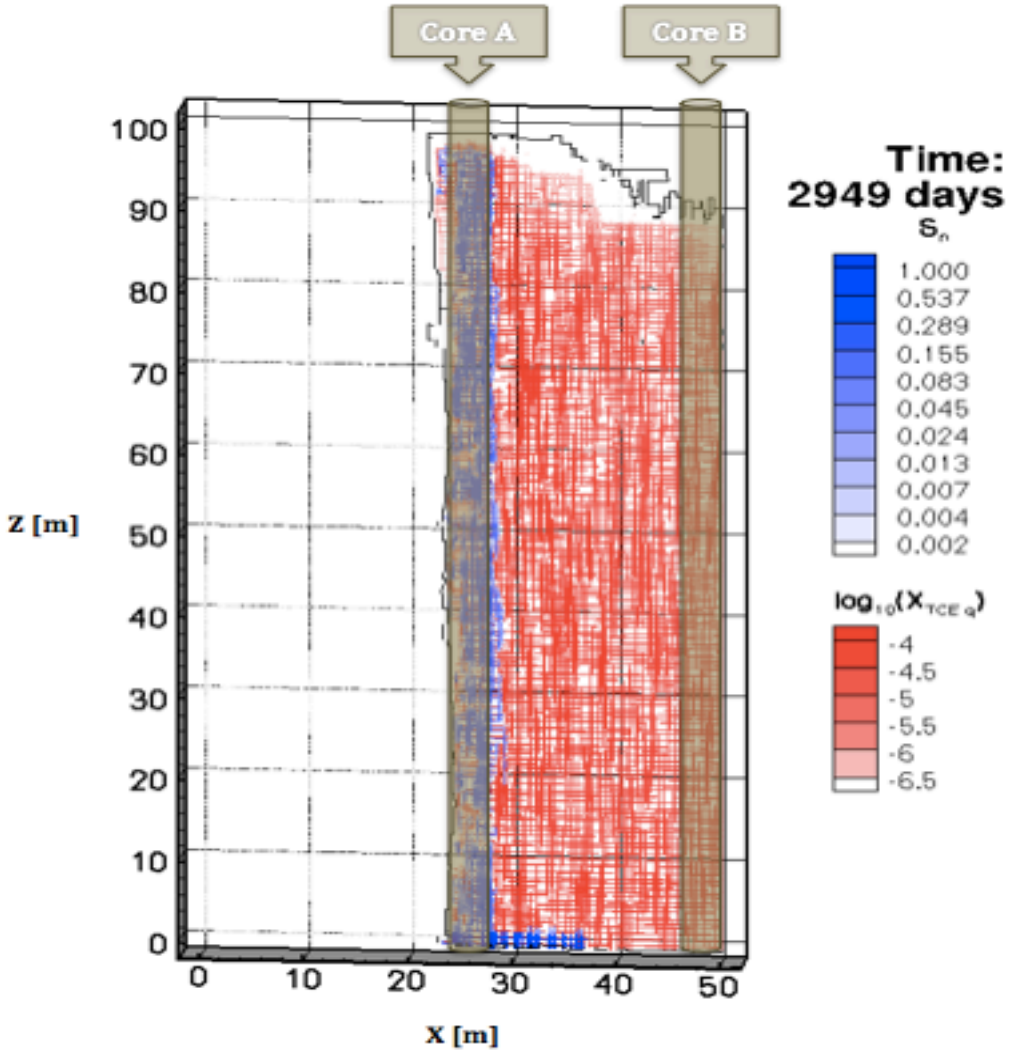

Figure 18 Conceptual model with virtual core setting of 2b=75μm case

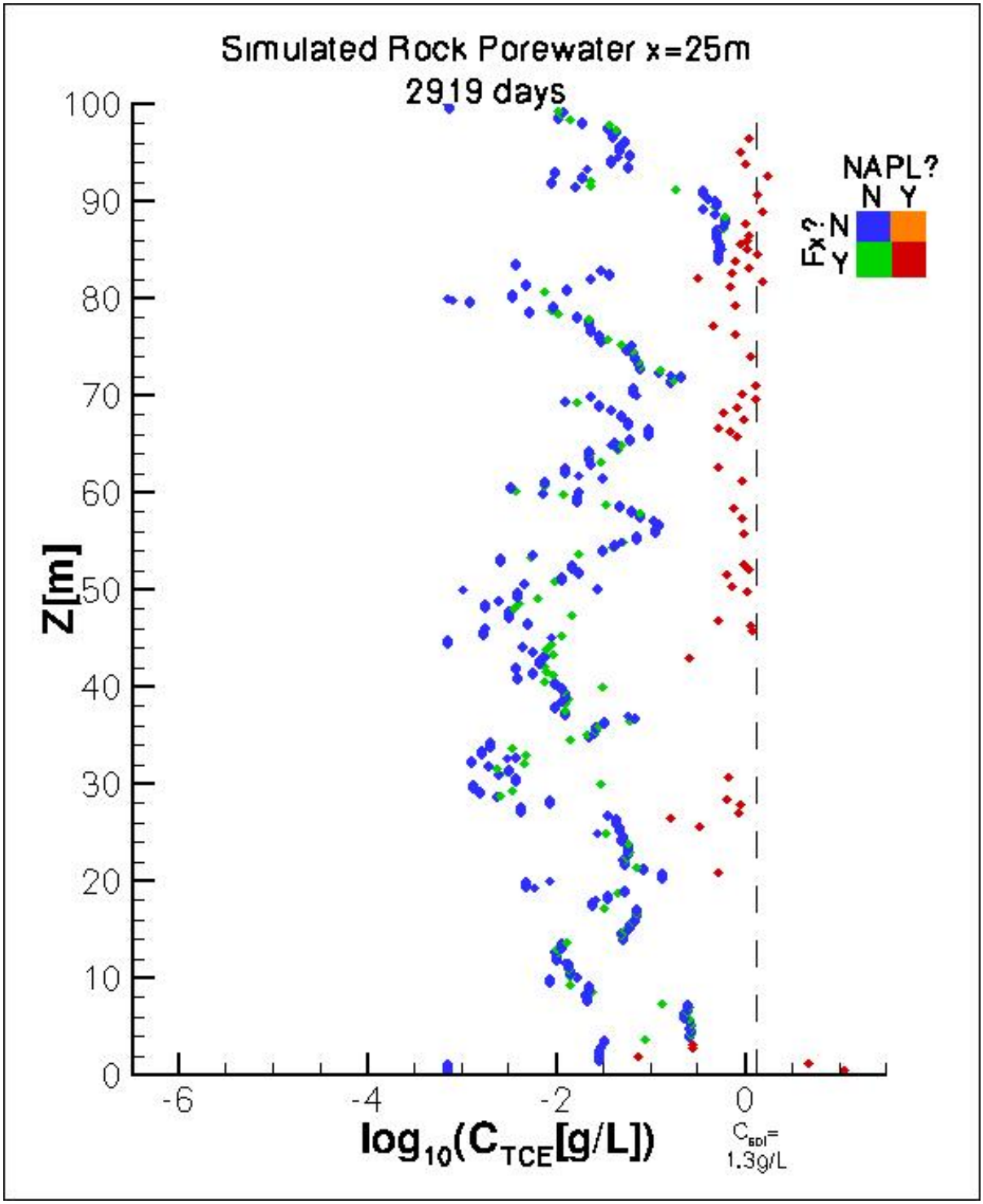

Figure 19 The virtual core sampling method of 2b=75μm case (Core through the middle axel at 8 simulation years)

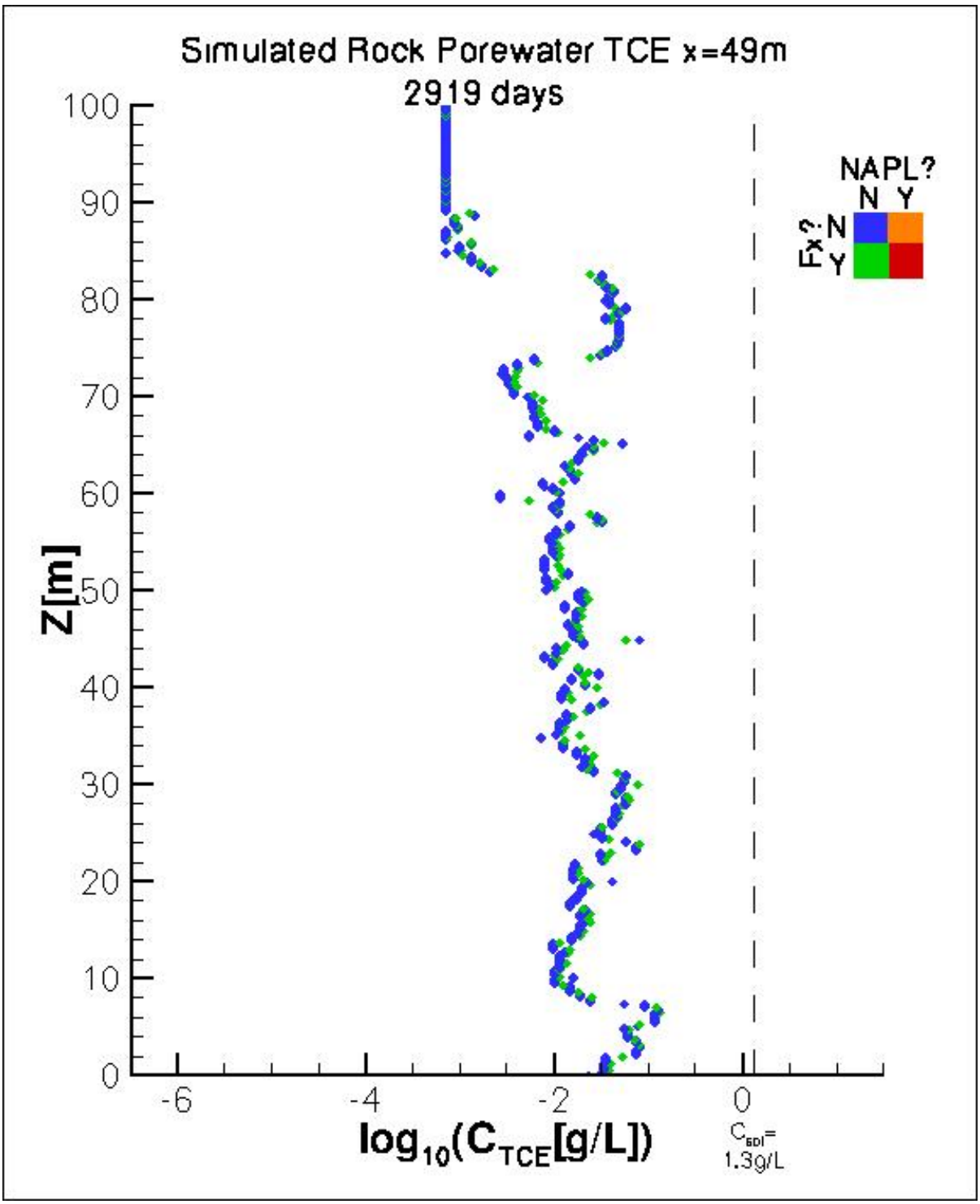

Figure 20 The virtual core sampling method of 2b=75μm case (Core through the outflow boundary at 8 simulation years)

Analyzing different phases of contaminant over time is another valuable approach to understand the fate of contaminant flow and transport. In Figure 21, the concentration of the NAPL phase of TCE (green curve), and the concentration the dissolved phase of TCE (red curve) are plotted over time. When TCE injected into the domain, it appears as NAPL phase and increase almost linearly until five days, when the concentration of the NAPL phase of TCE reach about 14kg; staying for about a month, the concentration of the NAPL phase of TCE slightly decreases. About 2 days after injection, part of TCE dissolved in water, and the concentration of dissolved phase of TCE increases over time. Observed from the 2b=100 μ m case, the concentration of NAPL and aqueous phase of TCE equaled to each other when the simulation ran to about 11 years; and then, the concentration of NAPL continuous to drop while the aqueous phase continuous to rise.

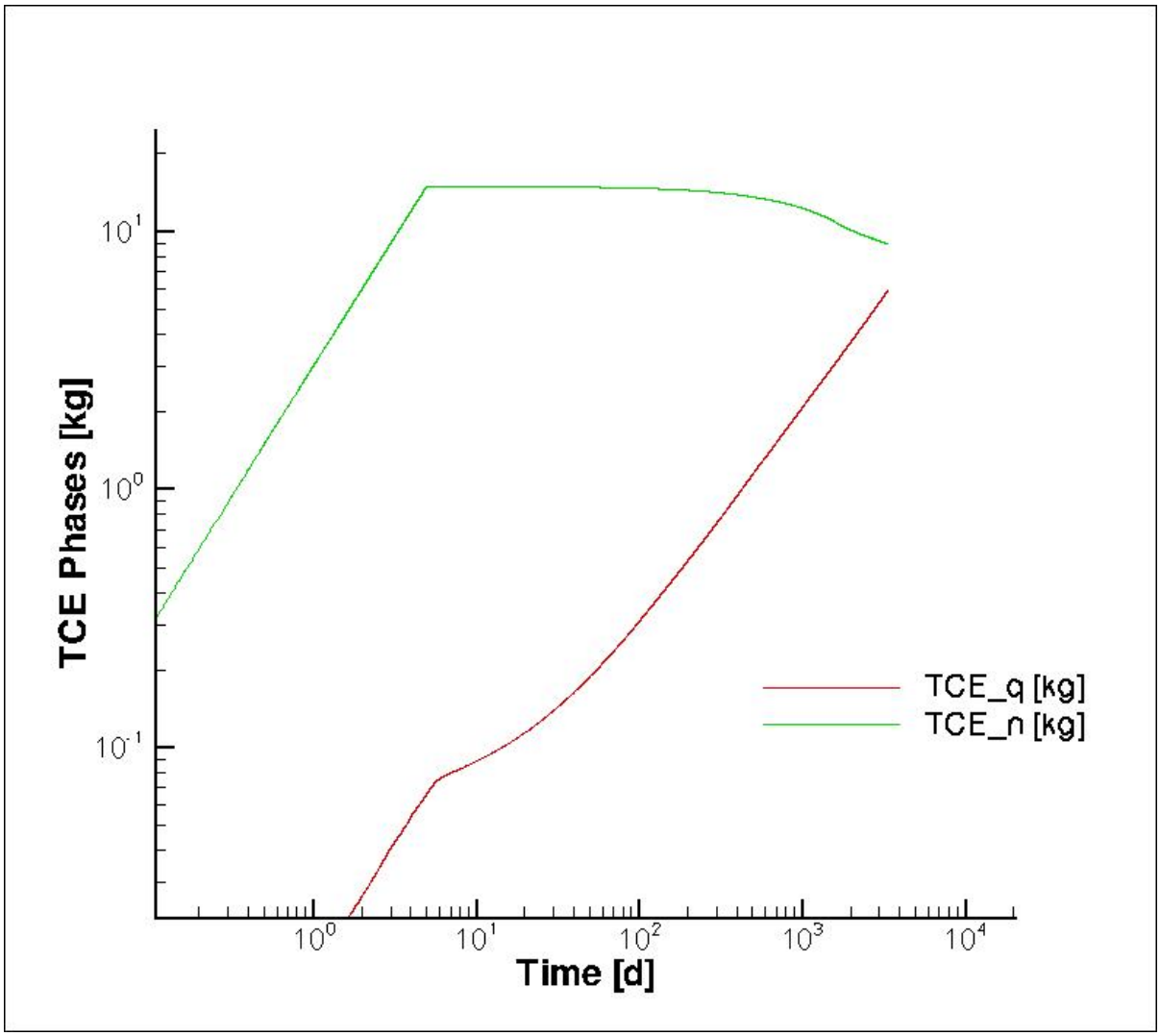

2b = 75 μ m

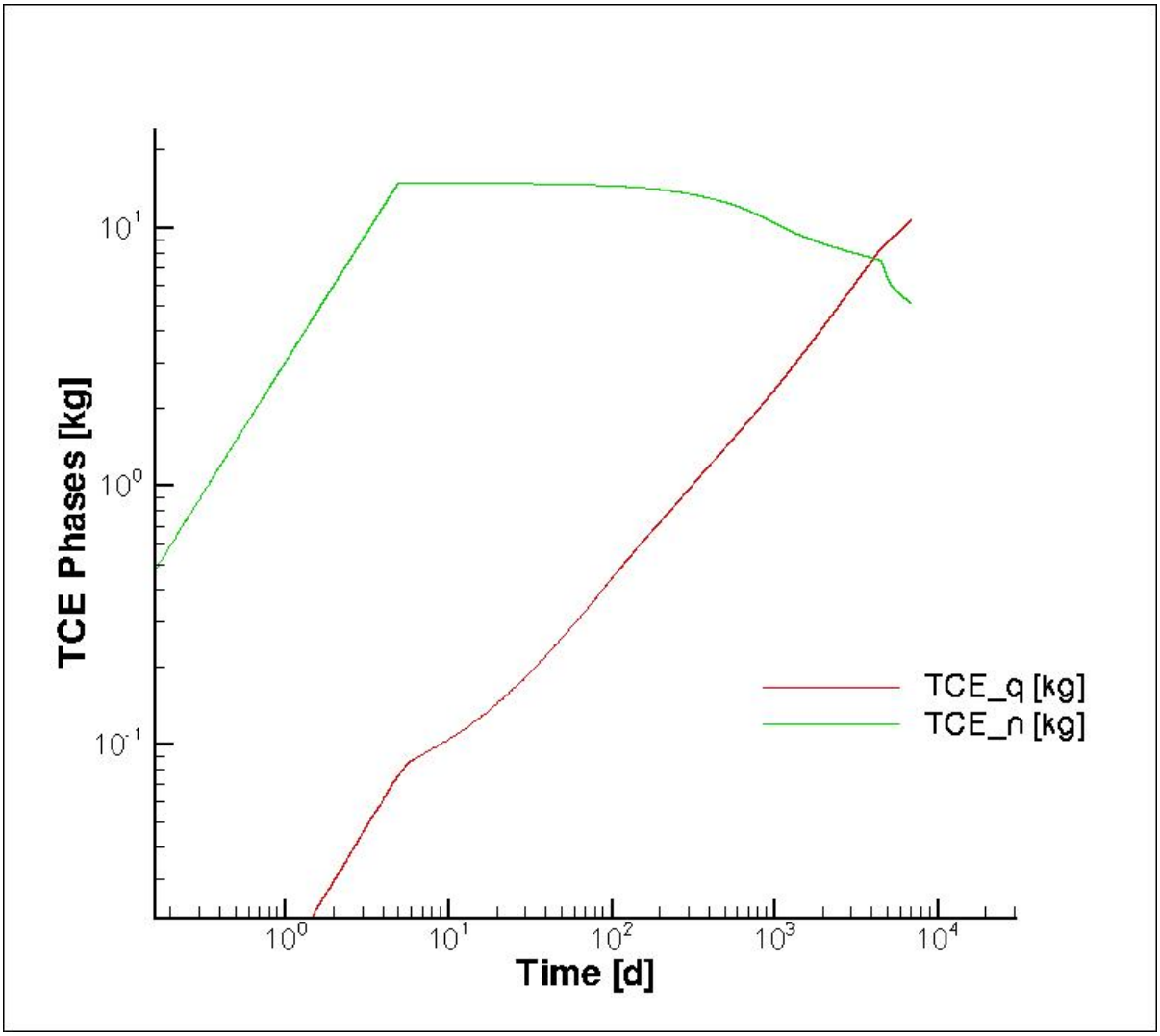

2b = 100 μ m

Figure 21 Longevity of TCE phases in the source zone with different fracture aperture size domain

4.4 Behavior of TCE transport though matrix and fracture

Mass flux of TCE over time though matrix and fracture of the domain are analysis near the outflow boundary as shown on Figure 22. TCE primarily and mainly transport through factures; the mass flux of TCE sharply increases from the beginning till about 30 days, and then the increase rate slows down, and after about 300 days, the mass flux of TCE almost stops to increase. After about 40 days, TCE begins to transport through pores media and the mass flux of TCE increases with fluctuation at the beginning and then increases smoothly and sharply.

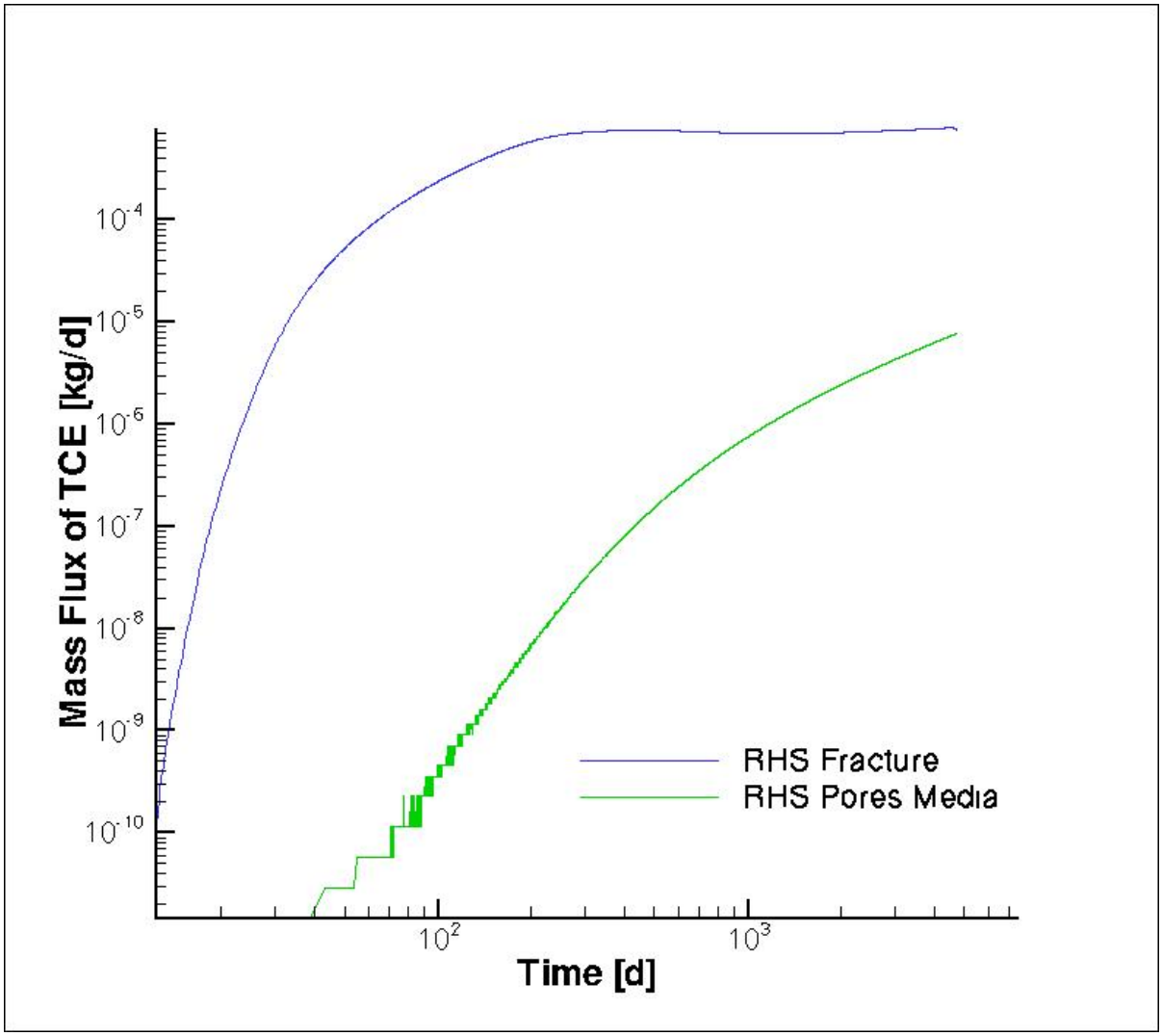

2b = 75 μ m

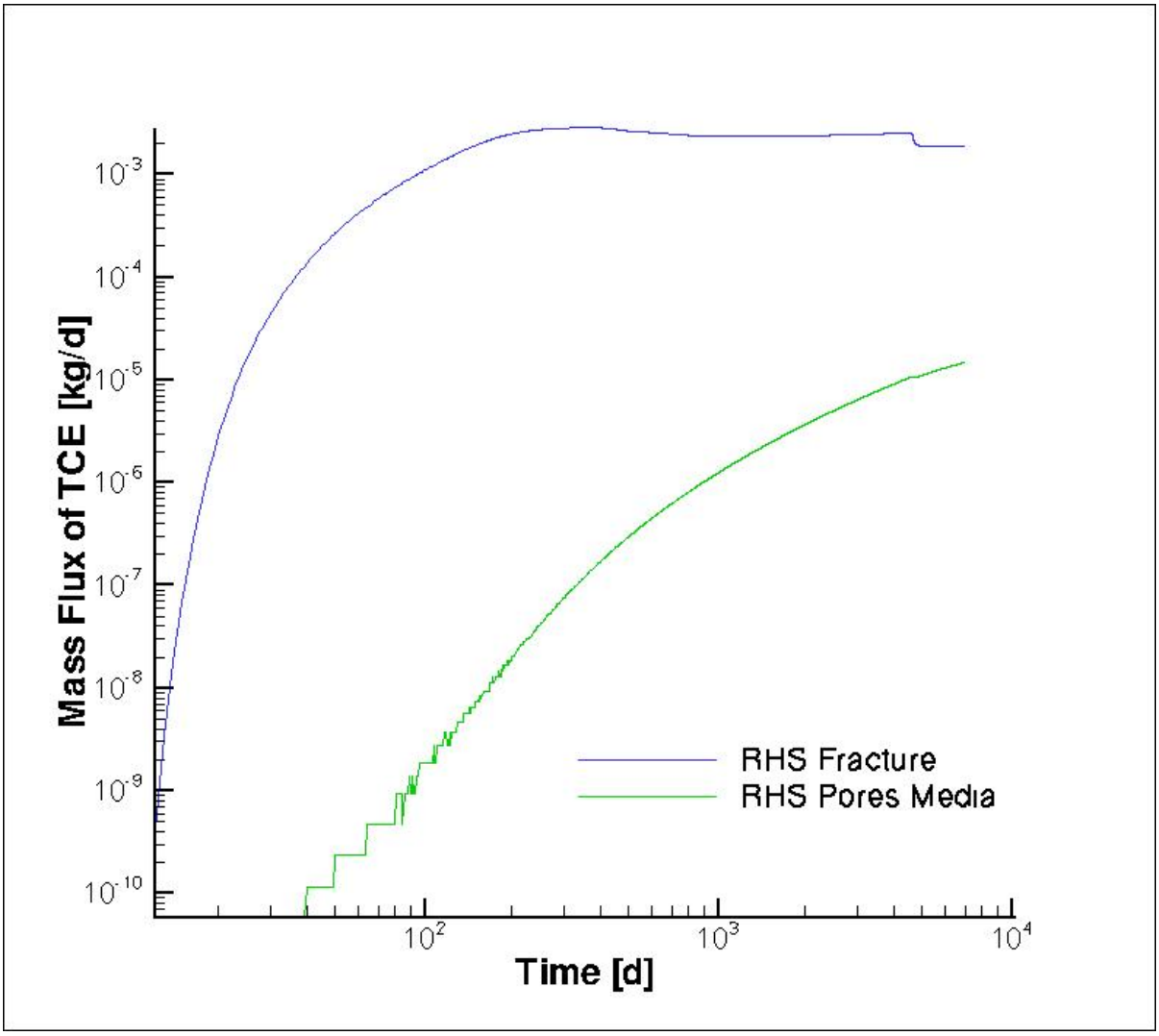

2b = 100 μ m

Figure 22 Mass flux of TCE through fracture and matrix in the source zone with different fracture aperture size domain

Chapter 5

Three Dimensional Numerical Model

5.1 Domain description

With the achievement of 2D numerical model, we try to increase our knowledge of the TCE flow and transport habit under groundwater flow conditions in a 3D domain. However, the domain size is restricted due to computational limits; we started with a 3D domain with 5m x 5m x 15m in x-, y- and z- directions, to simulate two- phase fluid (water and TCE) in medium. Same as in the 2D simulation model, the domain is set several meters below the water table (saturated without air phase). The simulation domain is shown on Figure 23. The fractures feature in this simulation is basely maintain the features tested from the sample at the SSFL. In this 3D domain, the fractures are distributed in xz-, yz- and xy- directions, and there are about 260 fractures in total. The aperture of fractures in the domain is set to be 75um and the density of fractures is set as approximate 3 per meter. In the domain, the permeability of fracture is about $5x10^{-10}$m2, and the permeability of matrix is about $1x10^{-15}$m2.

Different from 2D simulation model, there is no recharge in the 3D domain; But TCE load is applied on a small area at the top of the domain, with setting the permeability and porosity of porous media at the top greater than the rock matrix to permit down flow direction, TCE primarily dominate the vertical flow path. Another important condition is the lateral groundwater flow. To maintain a constant pressure conditions for natural groundwater flow, two thin fractures (red and blue planes) are settled on both left and right side. On the left side, an injection well injects water into the fracture at the bottom of the fractures; on the other side, a pumping well is set at the bottom of the fracture. The combination of the two wells can force a lateral groundwater condition with constant pressure, which is called steady state.

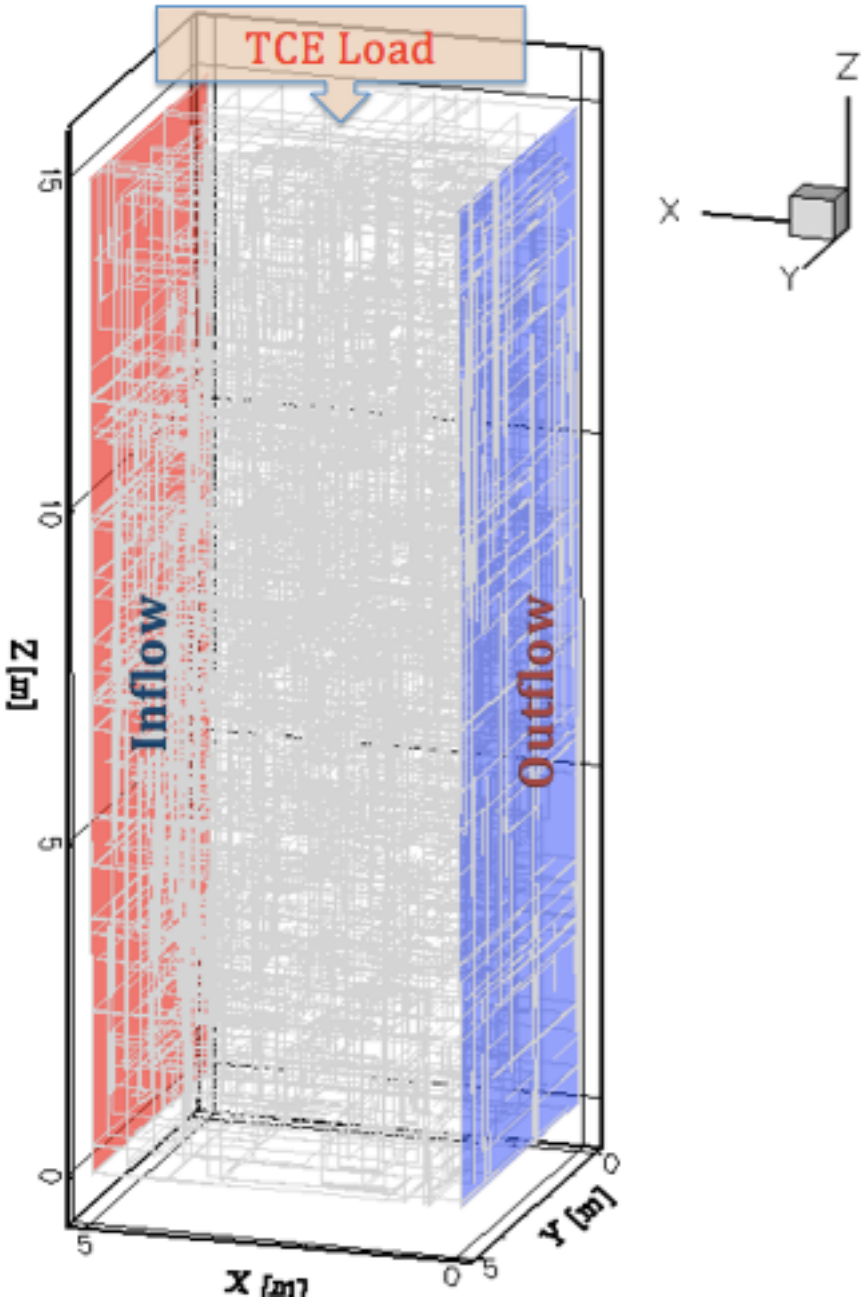

Figure 23 Boundary condition setting in the 5mx5mx15m domain conceptual model.

However, the injection rate of the injection well is required to be carefully determined to maintain the 1% hydraulic gradient for 2D TCE infiltrate simulation. An example of the wells setting in this case by CompFlow is shown in Figure 24. Well 1 in the injection well on the left boundary

injects water at a constant rate of 0.164408 m3/day, while the pumping well 3 is set on the right side with a constant pumping rate at 0.164419 m3/day. Because an issue with the code, it never gets to a "perfect" steady sate; and with the 0.4L/d (0.0004m3/d) difference allowance, this combination of an injection well and a pumping rate forces the later water flow under constant pressure head gradient.

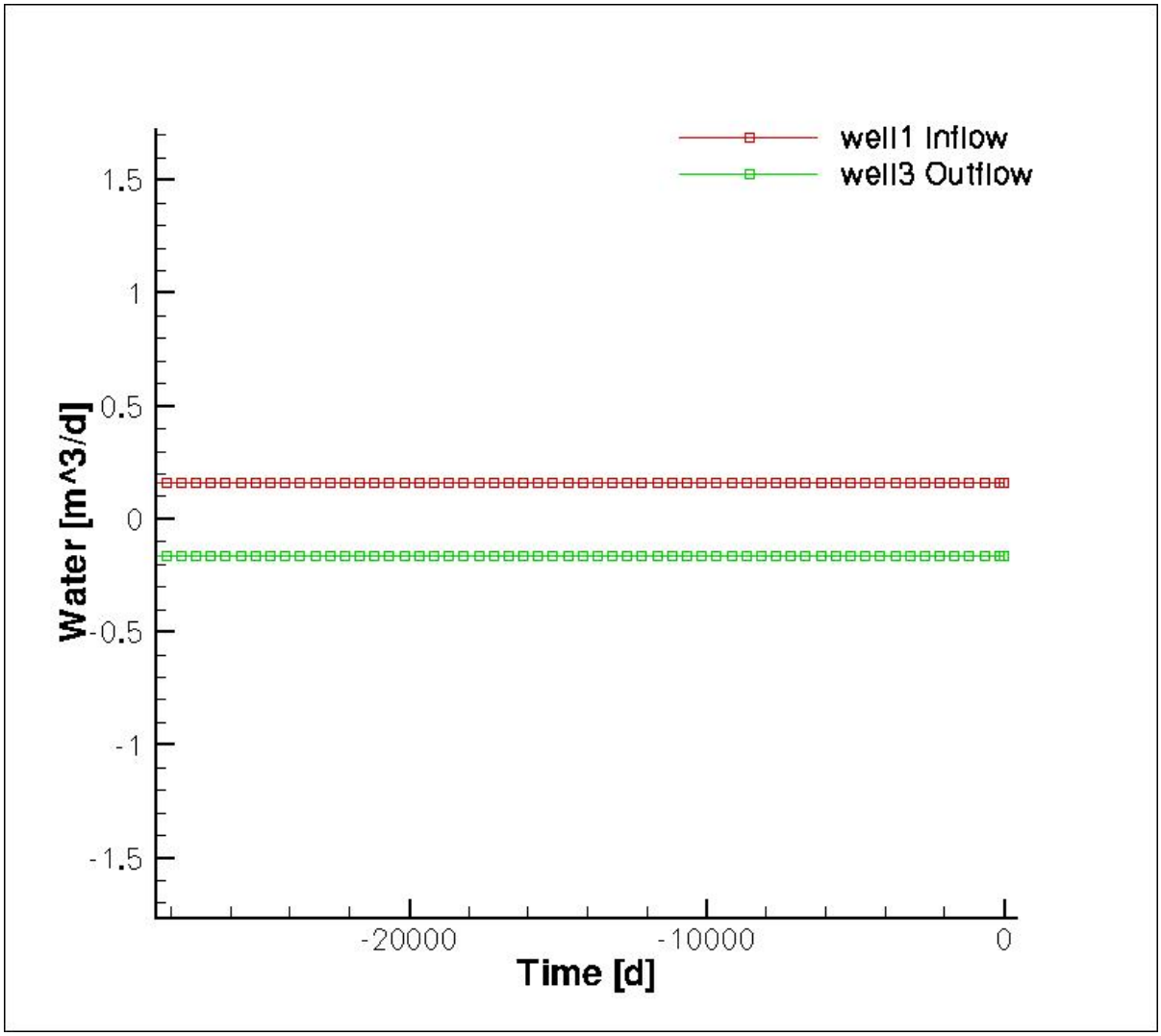

Figure 24 Water injection/pumping versus time, an example to illustrate how the wells settle the boundary conditions

The bulk hydraulic conductivity can be estimated with Darcy's Law once the domain reach the steady state:

$$K_{bulk} = \frac{Q}{A \times i} = \frac{0.1644\, m^3/day}{(15m \times 5m) \times (0.01)}$$

$$= 0.2192 m/day \; = 2.537 \times 10^{-6} m/s$$

K_{bulk} : The bulk hydraulic conductivity [m/s]

Q : Flow rate [m^3/day]

A : The area where the fluid flow through [m^2]

i : Hydraulic gradient [-]

Table 4 The bulk hydraulic conductivity with different apertures in 3D simulations

2b [um]	**Q[m^3/ day]**	**K_{bulk}[m/s]**
75	0.16439	2.54E-06
100	0.29121	4.49E-06
125	0.52722	8.14E-06
150	0.91752	1.42E-05

Figure 25 presents the relations between fracture aperture and bulk hydraulic conductivity estimates from 3D simulations. And the trend line estimated from this curve is about:

$$K_{bulk} = C \cdot (2b)^3$$

K_{bulk} : The bulk hydraulic conductivity [m/s]

C : A constant estimated from curve [-]

$2b$: Fracture aperture [um]

And this relationship between fracture aperture and bulk hydraulic conductivity is very similar to the cubic law (Snow, 1969) assuming that the hydraulic conductivity of the blocks of clay between the fracture is negligible.

$$(2b) = [\frac{K_{bulk} \cdot 2B \cdot 6 \cdot \mu}{\rho \cdot g}]^{\frac{1}{3}}$$

Recalculate K, the cubic law can present as:

$$K_{bulk} = [\frac{\rho \cdot g}{2B \cdot 6 \cdot \mu}]^3 \cdot (2b)^3 = C \cdot (2b)^3$$

K : Hydraulic conductivity [m/s]

$2B$: Fracture spacing [m]

μ : Dynamic viscosity of water [Pa s]

ρ : Density of water [kg/m^3]

g : Force due to gravity [N/kg]

$2b$: Fracture aperture [um]

C : A constant [-]

Therefore, based on the relations between fracture aperture and bulk hydraulic conductivity simulated from the 3D numerical model domain, the fluid is mainly flow through the fracture instead of the matrix in the domain.

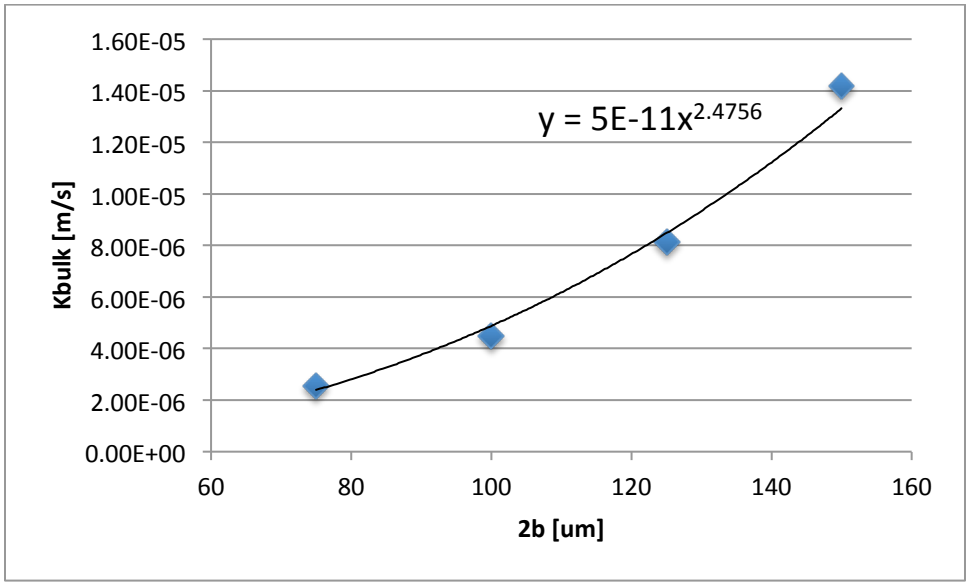

Figure 25 Relations between fracture aperture and bulk hydraulic conductivity in 3D simulations

5.2 Water/DNAPL simulation results in 3D domain

In this 5m x 5m x 15m 3D domain, the TCE is injected at 0.6 L/day in a small horizontal area on the top center of this domain, which just below the boundary layer, and below the water table. As mention in Chapter 4, about 2L/day of TCE is injected in a small horizontal area on the top center of the 50m x 0.3m x 100m 2D domain. Therefore, the size of 2D domain is about 4 times larger than the size of 2D domain, so TCE injected in the 2D domain is about 4 times of which in the 3D domain.

TCE is not expected to bind with soil particles or bioaccumulate. Since it is heavier than water and has a low solubility value, TCE is classified as a dense nonaqueous phase liquid, or DNAPL. This class of chemicals will tend to sink through a water column (both surface and ground) until they encounter a barrier that is sufficiently impermeable to stop them (Howard &Publishers, 1991). After 4 simulation days running (Figure 26), the NAPL of TCE reached the impermeable bottom boundary of the domain with fracture aperture sizes 75~150μm. Generally speaking, the infiltration flow dominants the TCE migration in saturated zone, and mainly in fracture network. The infiltration speed in vertical direction is pretty fast, approximate 3.75m/day (Figure 27).

Lateral advection under the natural groundwater floor condition is obvious with an approximate speed of 1m/day. The diffusion and dispersion transport is found in both matrix and fractures and in both vertical and horizontal directions.

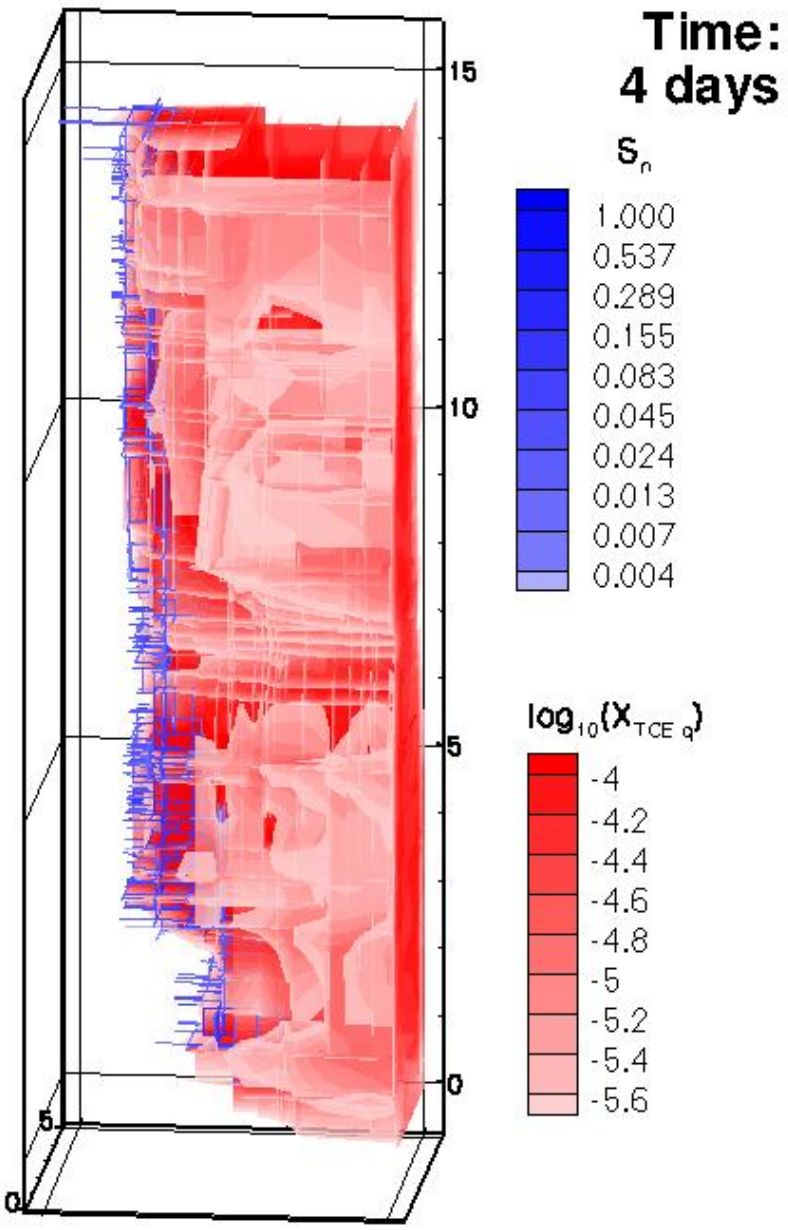

Figure 26 DNAPL and Plume Architecture of 2b=100µm case

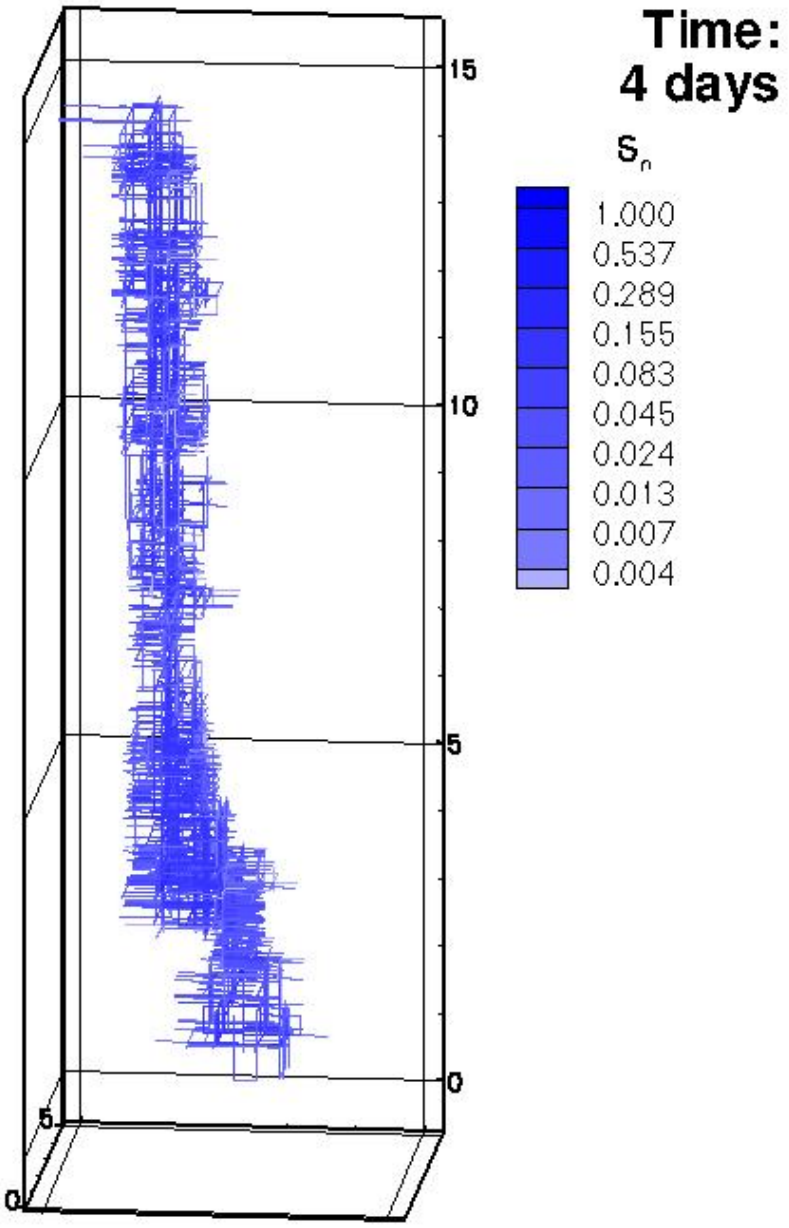

Figure 27 DNAPL Architecture of 2b=100μm case

5.3 The rock CORE^{TM} VOC method

In the 3D simulation, to assess the effects of diffusion of contaminants from fractures into the rock matrix, one virtual core is set to vertically penetrate through the middle axle of the domain at about x=2.5m.

Base on the sample data collected at SSFL via the rock CORE^{TM} VOC method, the distribution of TCE concentration among fracture and matrix at the virtual core location after 1 year simulation days and 50 years simulation days for a domain with 2b=100μm are present on Figure 28 and 29. In soils TCE often will leave a residual in pore spaces where the capillary pressure is strong enough to keep them from flowing. Once stopped, they and any residual will become a dissolved phase source for a very long time (Howard &Publishers, 1991). There are four cases for TCE to distribute in the domain: TCE appears as NAPL in both matrix (orange dot) and fracture (red dot), meanwhile, TCE dissolve in water and present in both matrix (blue dot) and fracture (green dot).

Comparing both graphs, some features can be summarized. After 1 year, TCE as NAPL phase is hardly detected even through the middle axel of the domain; the concentration of dissolved phase of TCE seems waveringly increases with depth from the top of the domain till about 10m deep, and then the concentration sharply decreases within about 1m to almost the minimum value. After 50 years, TCE are almost totally flushed away from the domain.

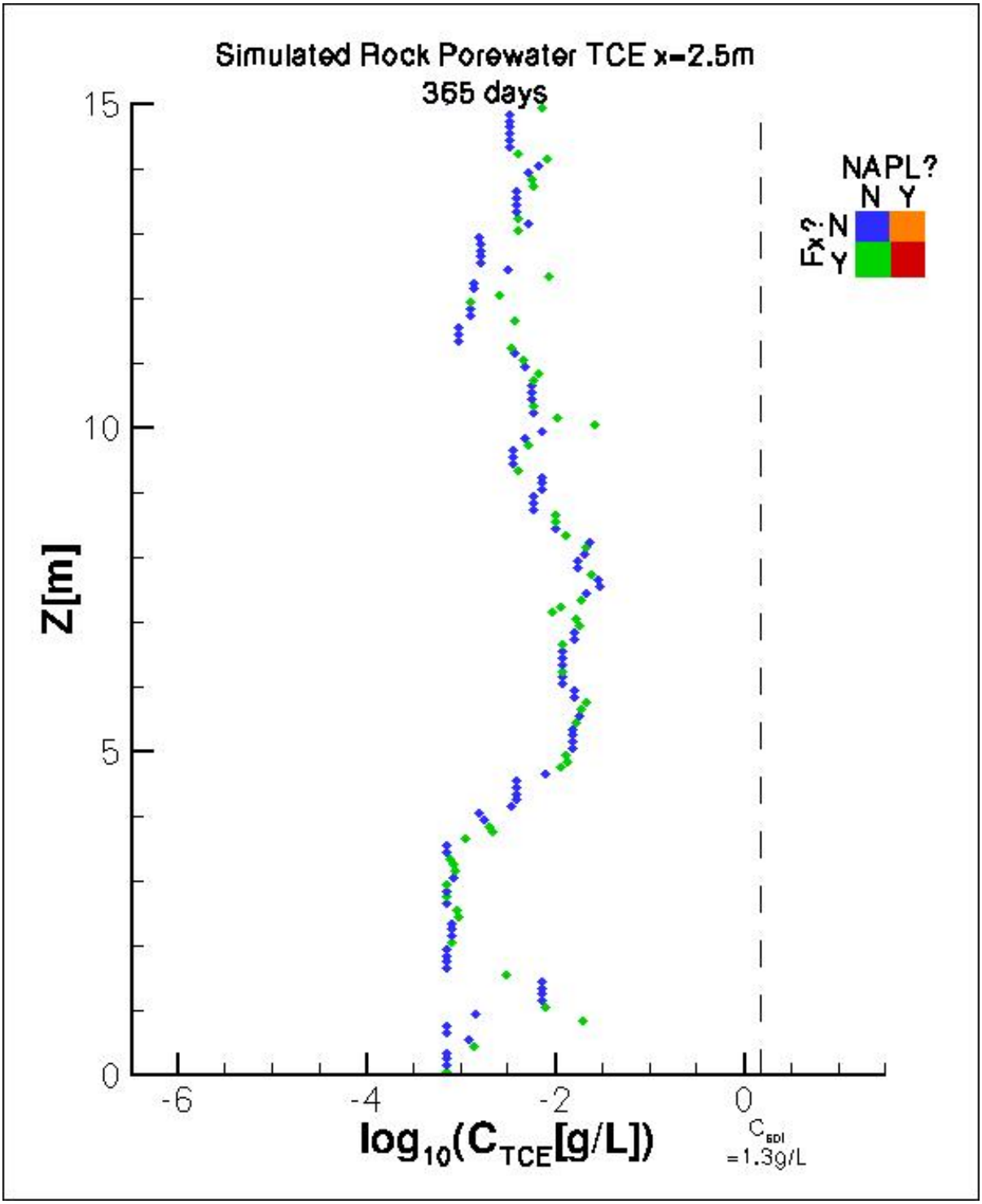

Figure 28 The virtual core sampling method of 2b=100μm case (Core through the middle axel at 1 simulation year)

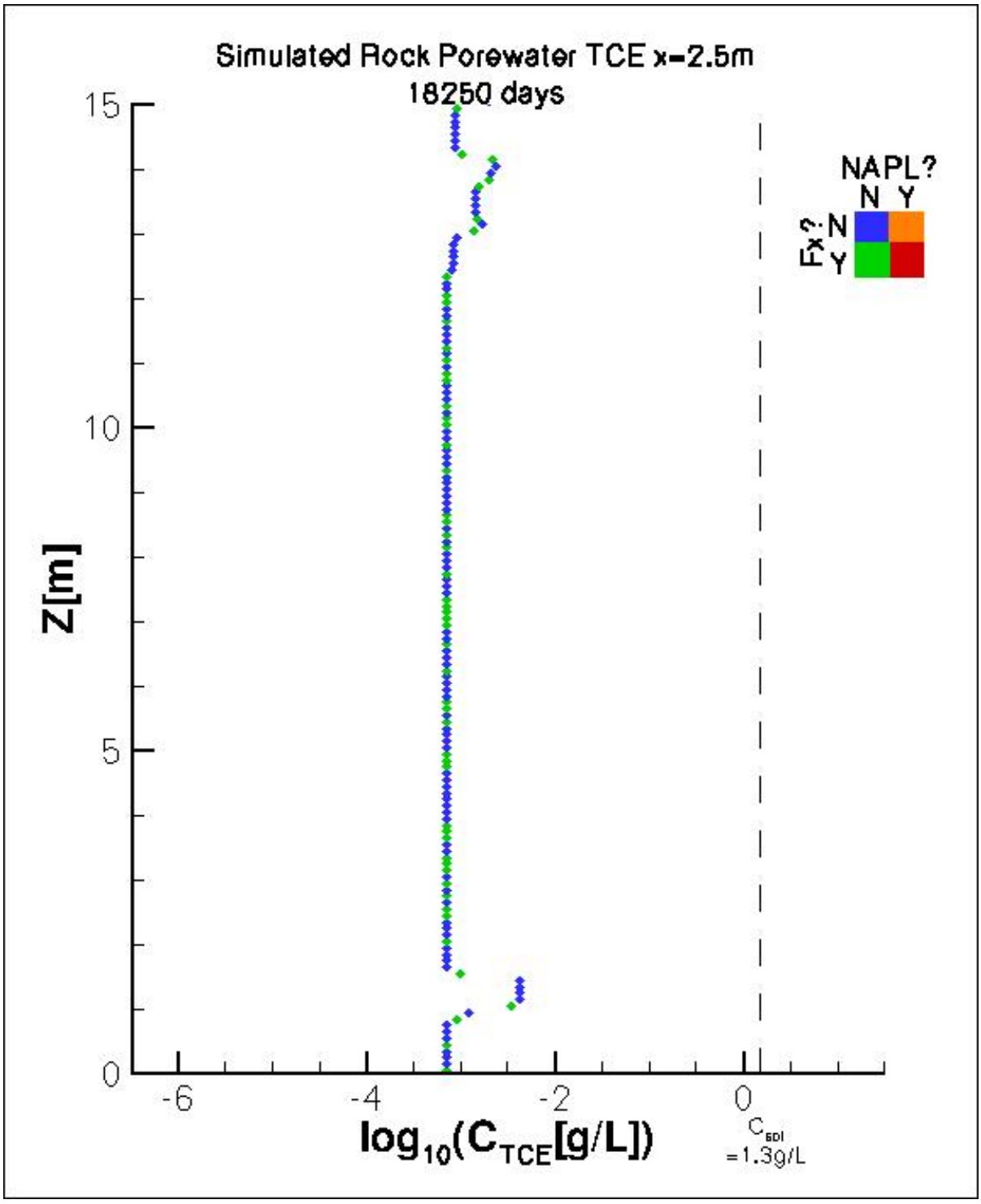

Figure 29 The virtual core sampling method of 2b=100μm case (Core through the outflow boundary at simulation 50 years)

5.4 Fate of TCE phases

Analyzing different phases of contaminant over time is another valuable approach to understand the fate of contaminant flow and transport. In Figure 30, the total concentration of TCE (pink curve), the concentration of the NAPL phase of TCE (green curve), and the concentration the dissolved phase of TCE (red curve) are plotted over time.

For all the four different 2b values fractured domain, when TCE injected into the domain, it appears as NAPL phase, and the concentration of both total and NAPL phase increase almost linearly until three days, when the total concentration of TCE reach about 2.3kg, and the concentration of the NAPL phase of TCE reach about 2.2kg; but after reaching the peak, the concentration for both the total and the NAPL phase of TCE slightly decrease, and the NAPL phase of TCE decreases more sharply, so that the green line slightly split from the pink one.

About 2 days after injection, part of TCE dissolved in water, and the concentration of dissolved phase of TCE increases almost linearly until almost the same time when the linearly increasing of the concentration of both total and NAPL phase stops. For 100μm ~150μm 2b values fractured domain, the linearly increasing of the concentration of dissolved phase stops at the peak where concentration of dissolved phase is about 0.1kg; after reaching the very narrow peak, the concentration of dissolved phase decrease also linearly until it meets the concentration of total TCE, and then, these two curve blend together and decrease with parabolic shape. But for the 75μm 2b values fractured domain, the increase rate slow down to reach the peak after the linearly increasing of the concentration of dissolved phase stops, and the peak concentration of dissolved phase of TCE for this case reaches about 0.13kg. And then, the concentration of dissolved phase meets the concentration of total TCE and these two curve blend together and decrease with parabolic shape. As shown on the Figure 31, simulations of 75μm ~150μm 2b values fractured domain are finished, and all the TCE including NAPL phase and dissolved phase are flushed out of the domain.

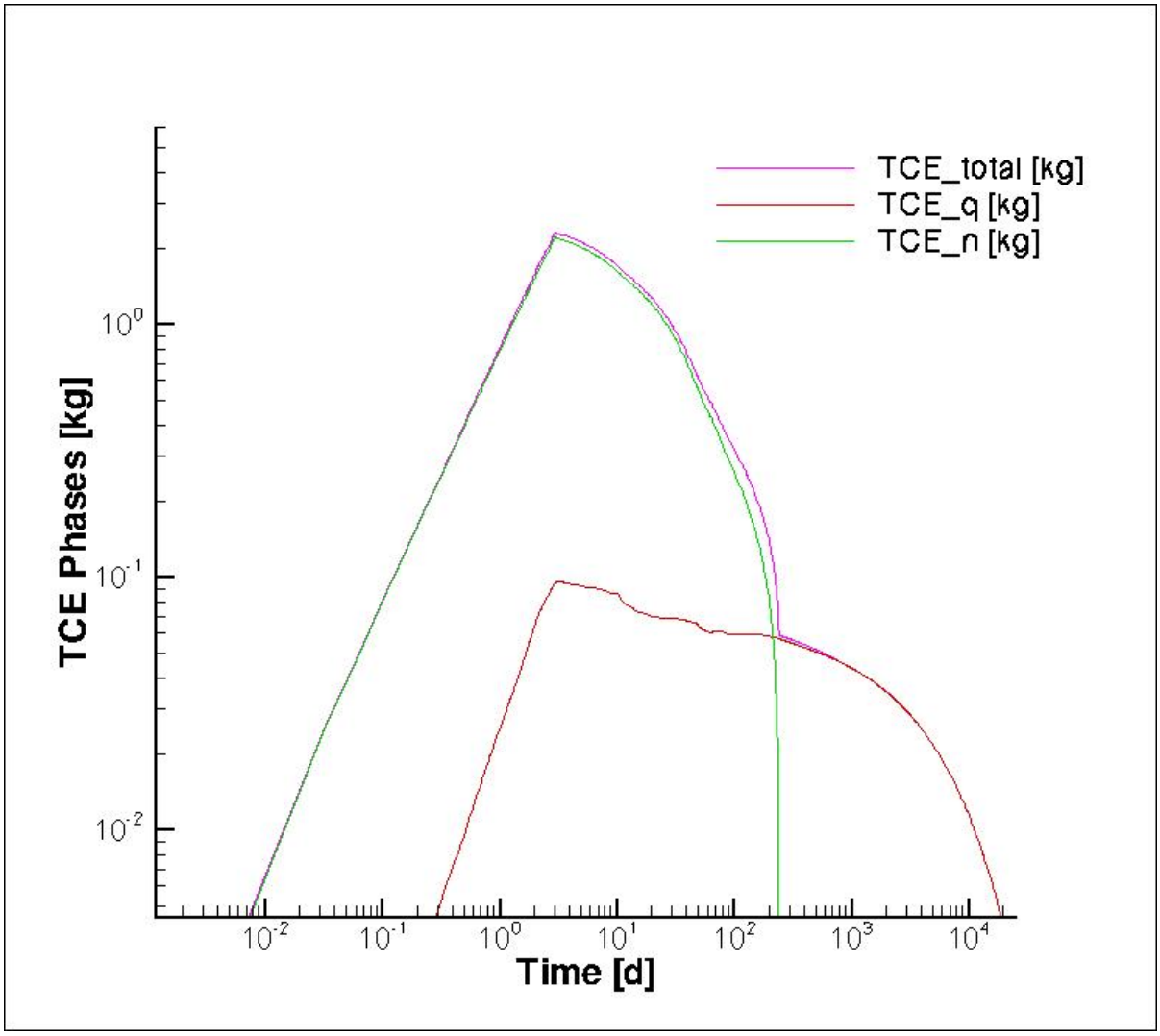
TCE_total [kg]
TCE_q [kg]
TCE_n [kg]
TCE Phases [kg]
10^0
10^-1
10^-2
10^-2
10^-1
10^0
10^1
10^2
10^3
10^4
Time [d]

2b = 75 µm

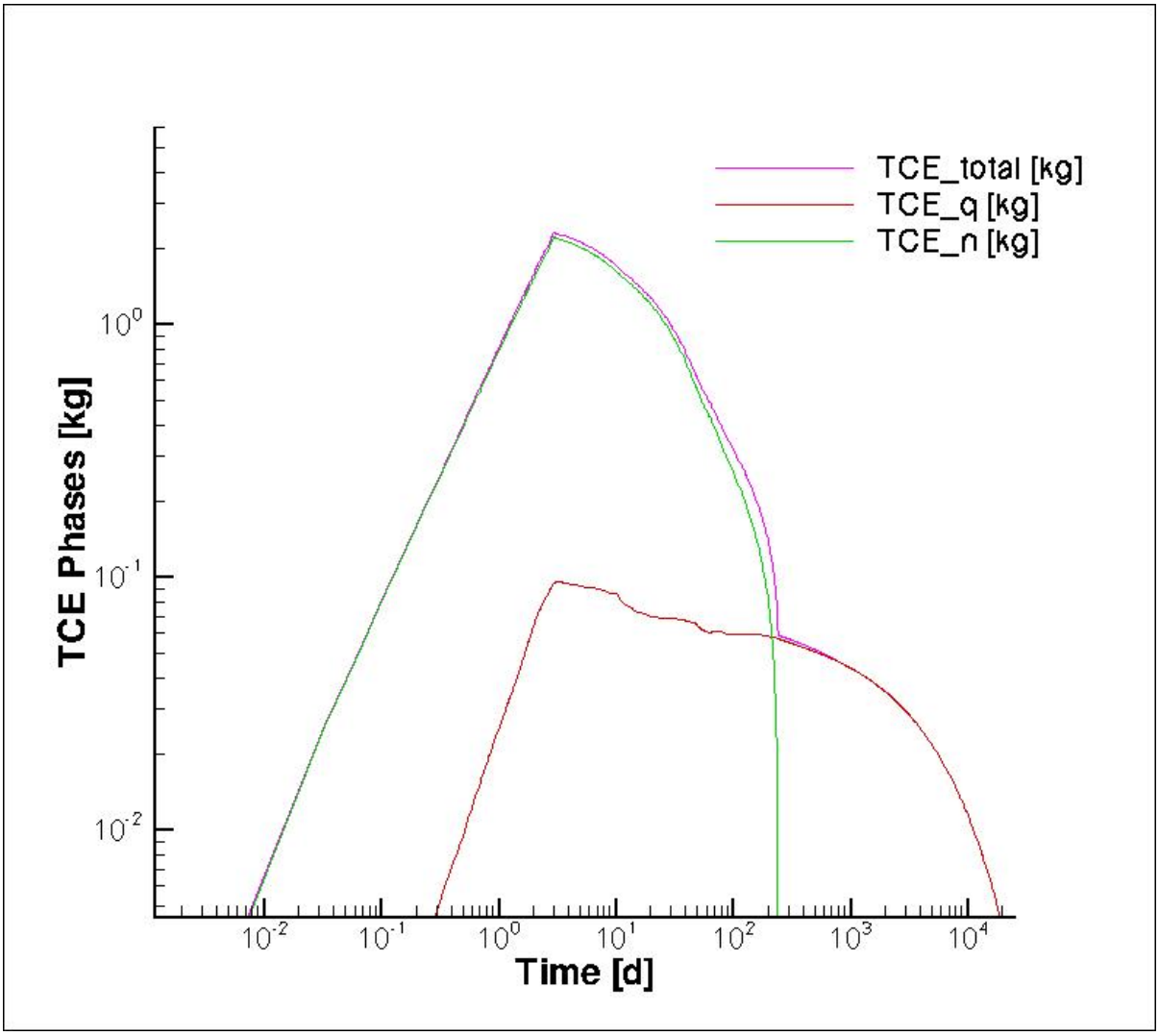
TCE_total [kg]
TCE_q [kg]
TCE_n [kg]
TCE Phases [kg]
10^{0}
10^{-1}
10^{-2}
10^{-2}
10^{-1}
10^{0}
10^{1}
10^{2}
10^{3}
10^{4}
Time [d]

2b = 100 µm

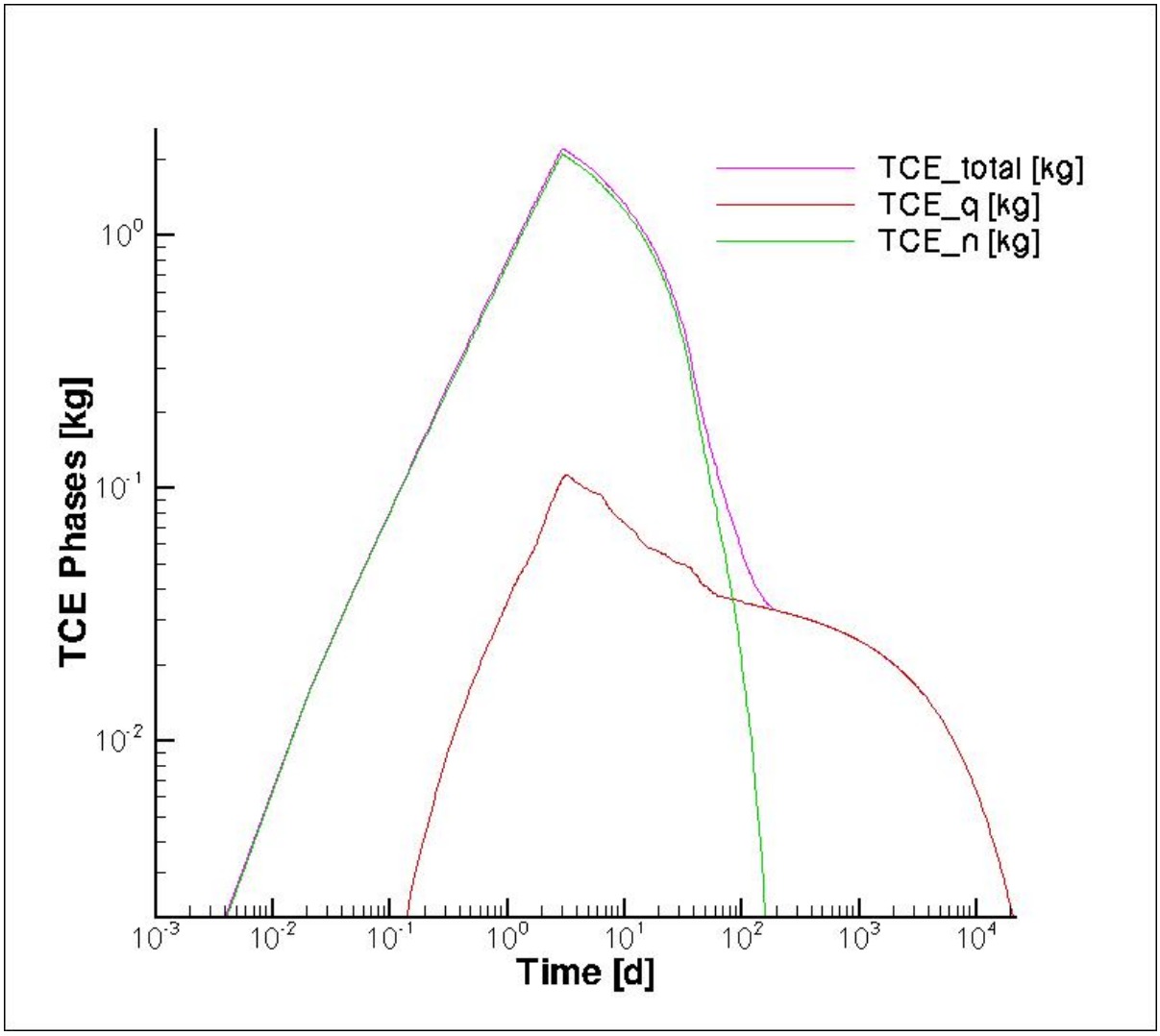
TCE_total [kg]
TCE_q [kg]
TCE_n [kg]
TCE Phases [kg]
10^{0}
10^{-1}
10^{-2}
10^{-3}
10^{-2}
10^{-1}
10^{0}
10^{1}
10^{2}
10^{3}
10^{4}
Time [d]

2b = 125 µm

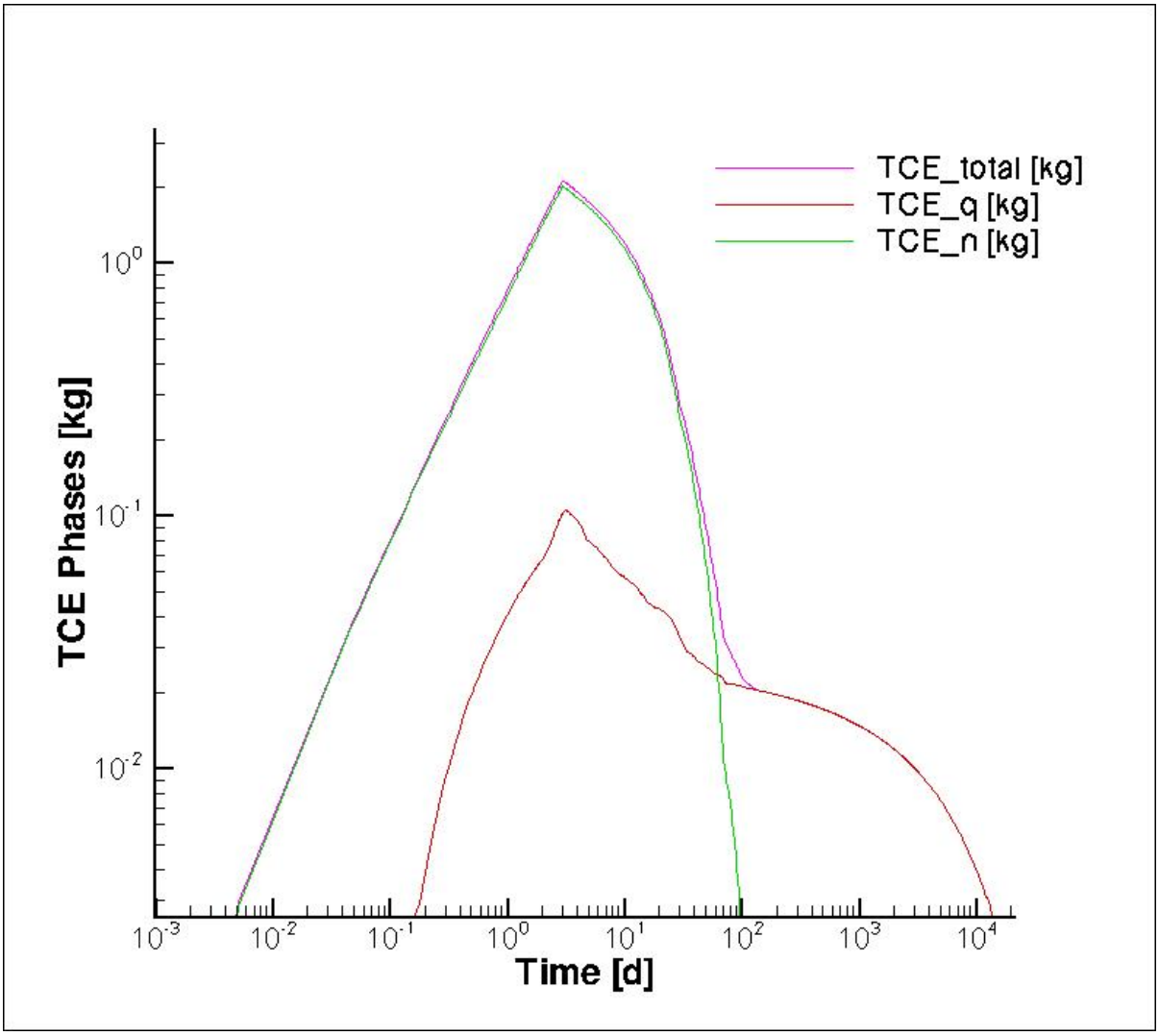

2b = 150 µm

Figure 30 Longevity of TCE phases in the source zone with different fracture aperture size domain

5.5 Behavior of TCE transport though matrix and fracture

Mass flux of TCE over time though matrix and fracture of the domain are analysis near the outflow boundary as shown on Figure 30. TCE primarily and mainly transport through factures; the mass flux of TCE draws a parabolic curve till about 200 days, and then decreases almost linearly after that, and at about 5 days the parabolic curve reach the peak where the mass flux of TCE through fractures is about 0.6kg/d. After about only 0.2 day, TCE begins to transport through pores media and the mass flux of TCE also draws a parabolic curve, and it reaches the peak where the mass flux of TCE

through fractures starts to decrease near linearly. Is very obvious to tell from the figure 31 that the mass flux through fractures is much more than that through the matrix; moreover, the amount of mass flux through the matrix decreases as the fracture aperture size increases, because water is easier to flow through larger fracture. Simulations of 100μm ~150μm 2b values fractured domain are finished, but maybe due to narrower fracture size restricting the TCE, the simulation of 75μm 2b values fractured domain have not yet but almost finished.

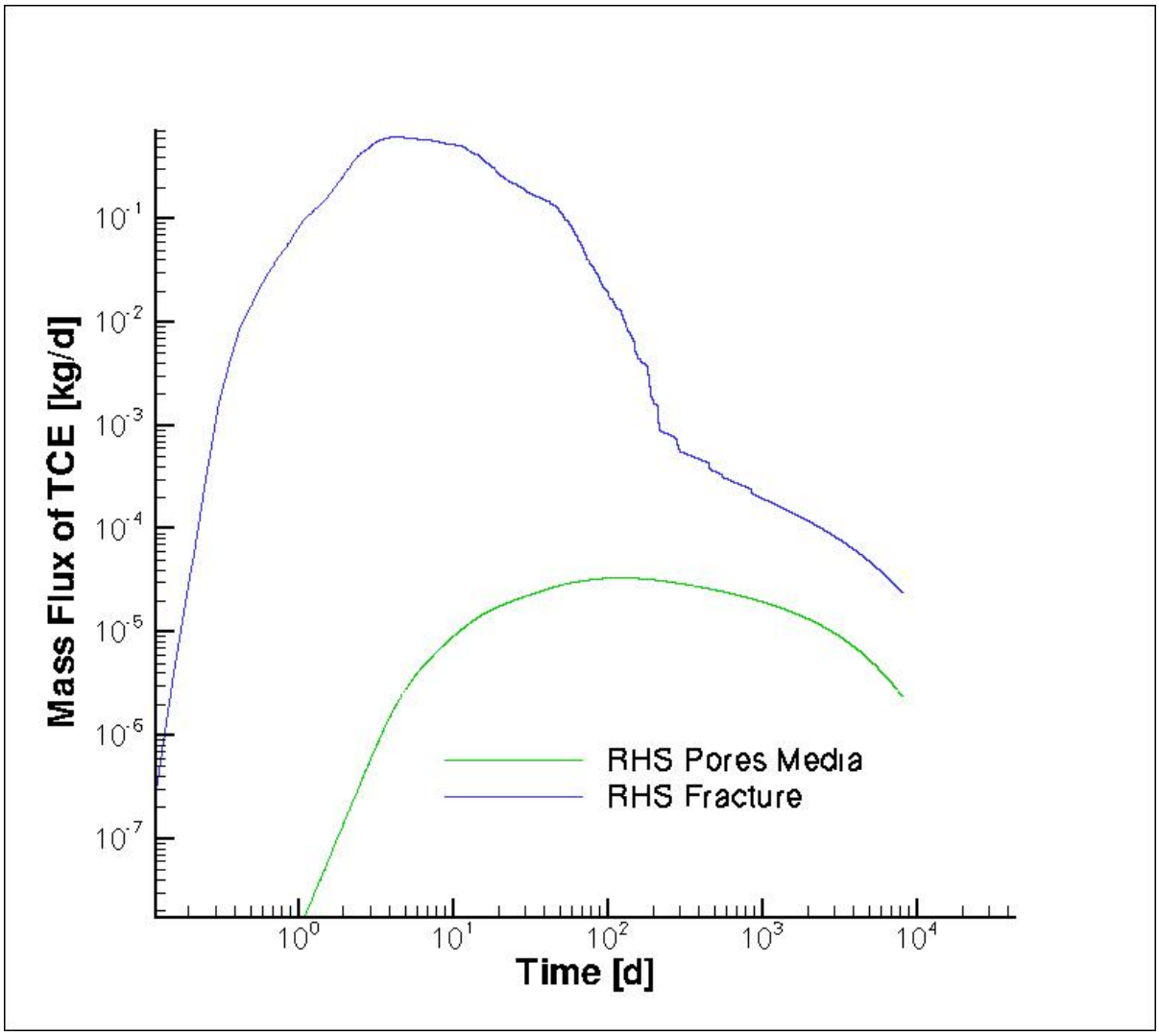

2b = 75 μm

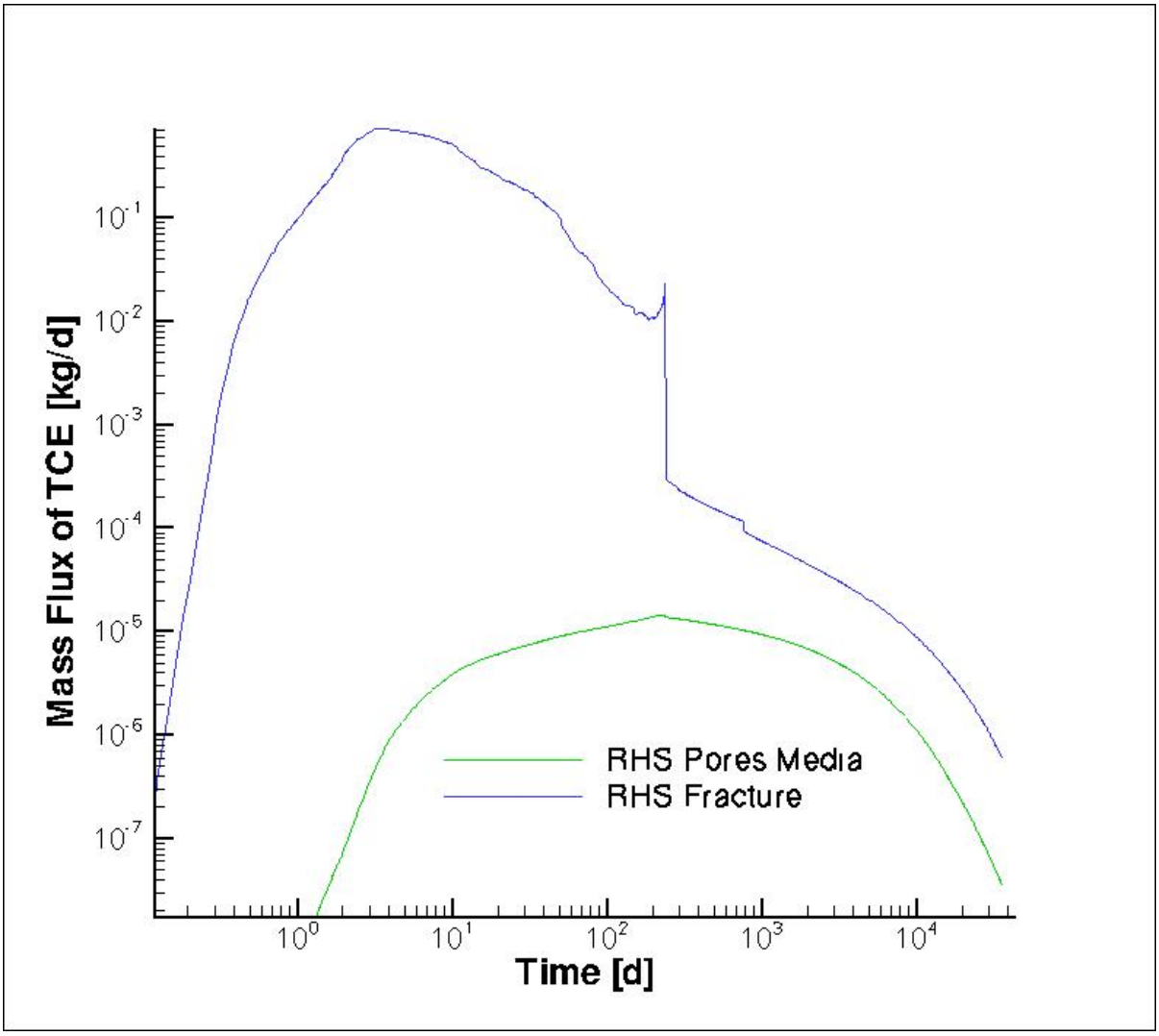
Mass Flux of TCE [kg/d]
10-1
10-2
10-3
10-4
10-5
10-6
10-7
RHS Pores Media
RHS Fracture
100
101
102
103
104
Time [d]

2b = 100 µm

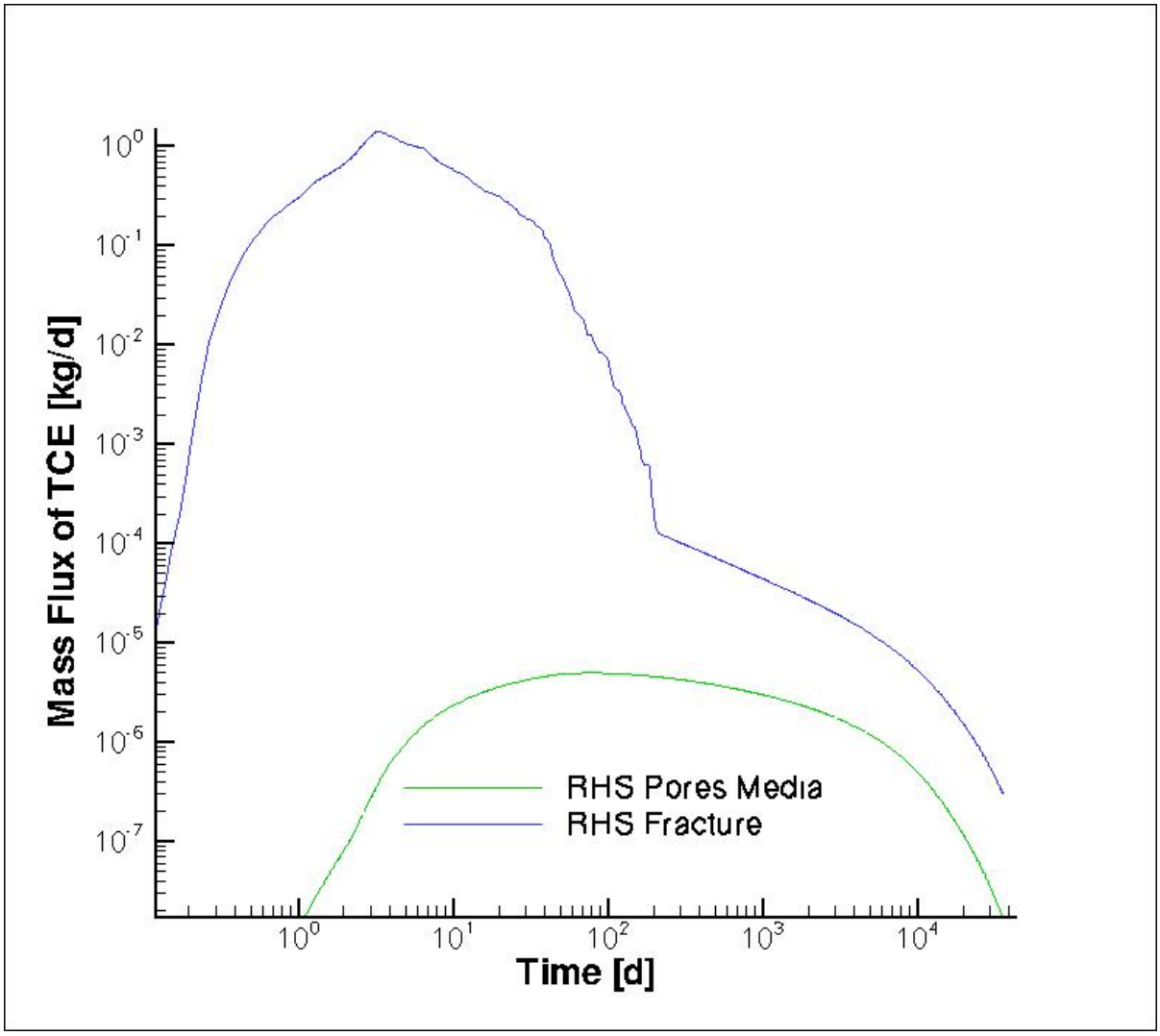
Mass Flux of TCE [kg/d]
10^{0}
10^{-1}
10^{-2}
10^{-3}
10^{-4}
10^{-5}
10^{-6}
10^{-7}
RHS Pores Media
RHS Fracture
10^{0}
10^{1}
10^{2}
10^{3}
10^{4}
Time [d]

2b = 125 µm

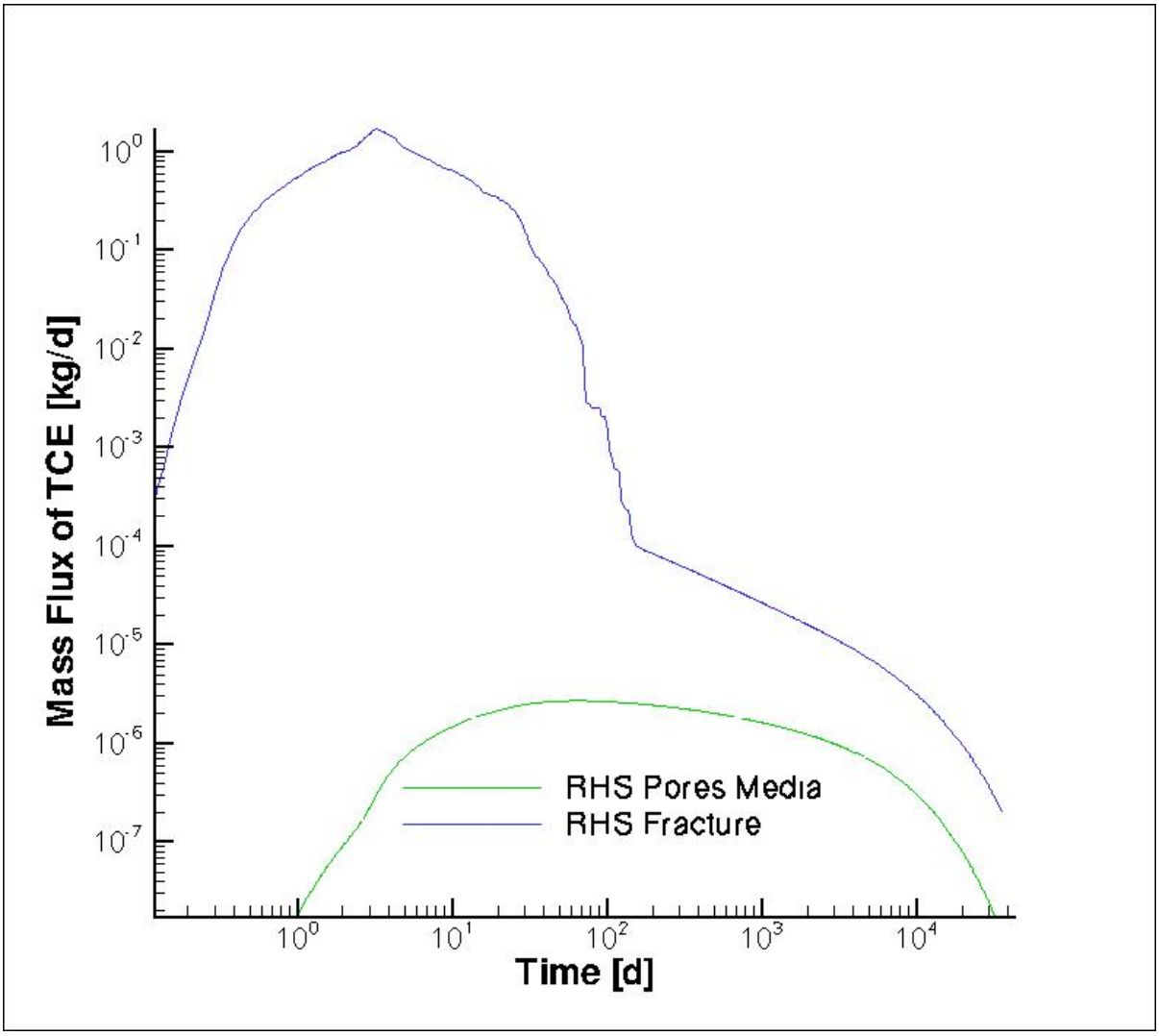

2b = 150 µm

Figure 31 Mass flux of TCE through fracture and matrix in the source zone with different fracture aperture size domain

Chapter 6

Conclusions and Recommendations

6.1 Summary

Due to industrial activities from 1940 through 1990, a toxic contaminant with low solubility in the water, TCE and its daughter products were introduced in the fractured bedrock with a turbidities sequence of sandstones with shale interbeds underneath the Santa Susana Field Laboratory (SSFL). For managing the contamination to protect the groundwater resource, several previous works on the site conceptual mode have been finished during the past decades of years. In this study, we employ the CompFlow Bio to build both 2D and 3D numerical model to find out: 1) if the DNAPL penetrated to 100 m below the ground surface at this site as previous works hypothesized; 2) how long it takes to dissolve away the DNAPL at this site; 3) how different are the manners of mass fluxing away from source zone by path of matrix and fracture.

Considering those three aspects listed above, we started with 2D numerical model whose domain size is 50m x 0.3m x100m to find out how long it take for DNAPL in source zone to dissolve away; and then, for represent more like the "real world", we applied these simulations on a 3D numerical model except that its domain size is restricted to be only 5m x5m x15m because of computational limits. According to the statistic data analysis of the drill cores analysis done by Cherry, McWhorter et al. 2009, the most proportion in both directions is 125 microns. In addition, 50~175 also get larger proportions of fracture apertures. Therefore, our original purpose is to use 75, 100, 125, 150 microns 2b values in both 2D and 3D conceptual model so as to determine the most reasonable 2b value for DNAPL simulation. But only 75 and 100 microns 2b value used in the 2D simulation due to computational limits, though all the microns 2b values used in the 3D simulation with smaller domain size.

For both 2D and 3D simulations in this study, the rock core VOC analyses of the source zone and outflow boundary (only for 2D domain) compared with field data from SSFL were discussed; and the mass flux of TCE in the aqueous phase exists the fence boundary in fracture and matrix was investigated.

6.2 Conclusions

Though the long-term run of 2D numerical simulations haven't been finished due to computational limits, some useful observations are achieved in this study. The bulk hydraulic conductivity estimated from the 2D domain is on the level of 10^{-7} m/s. The TCE contour plots of the 2D simulation clearly show that the NAPL tends to sink vertically right after they are loaded until they stopped by impermeable boundary, and this infiltration flow occurs mainly in fracture network with little no transverse spreading; but once stopped, the NAPL and any residual becomes a dissolved phase plume and fluxed with lateral groundwater flow. And this is also supported by the VOC method with coring vertically through the middle axle and outflow boundary of the domain.

Due to smaller size of the domain and smaller amount of TCE loaded into the domain, almost all the 3D simulations with different fracture aperture values were finished except the 75 microns 2b value case are coming to the end. The bulk hydraulic conductivity estimated from the 3D domain is on the level of 10-6 m/s, which is larger than that estimated from the 2D domain; and this is possibly because the 3D domain has more interconnected space allowing fluid to flow though while the 2D domain spatially restricts the flow. From the drill cores analysis, the bedding parallel fractures and joints are highly interconnected and form orthogonal fractures. The length of fractures is small to moderate with range from 0.5m to 20m (Cherry, McWhorter et al. 2009). The regional hydraulic data indicates the fractures effectively connect to other fractures creating the continuum of groundwater flow. Therefore, the 2D domain, to a certain extent, cutoff part of the fracture network and limits the flow through the domain, so that there less flow through the 2D domain than that through the 3D one. The plots of conversion among TCE phases over time in the 3D domain with different fracture apertures commonly present that NAPL is original dominant phase of TCE in the water, and then it tends to dissolve and so as to be finally fluxed out of the domain. Moreover, smaller fracture apertures have higher capillary pressure to keep the TCE from flowing, and thus, it takes more time for the concentration of dissolved phase TCE curve to reach the peak and then meet the total curve in smaller fracture aperture than that in larger fracture aperture. In addition, Flow through fracture is proved to be easier than that through matrix, and larger fractures become the main conduit.

6.3 Recommendations for Future Research

Sterling et al. (2005) made worthy comparison of rock-core data and multilevel ground water TCE concentrations (Figure 32), and the ground water TCE concentrations calculated by the virtual core sampling method maybe also worth to comparing to the field data.

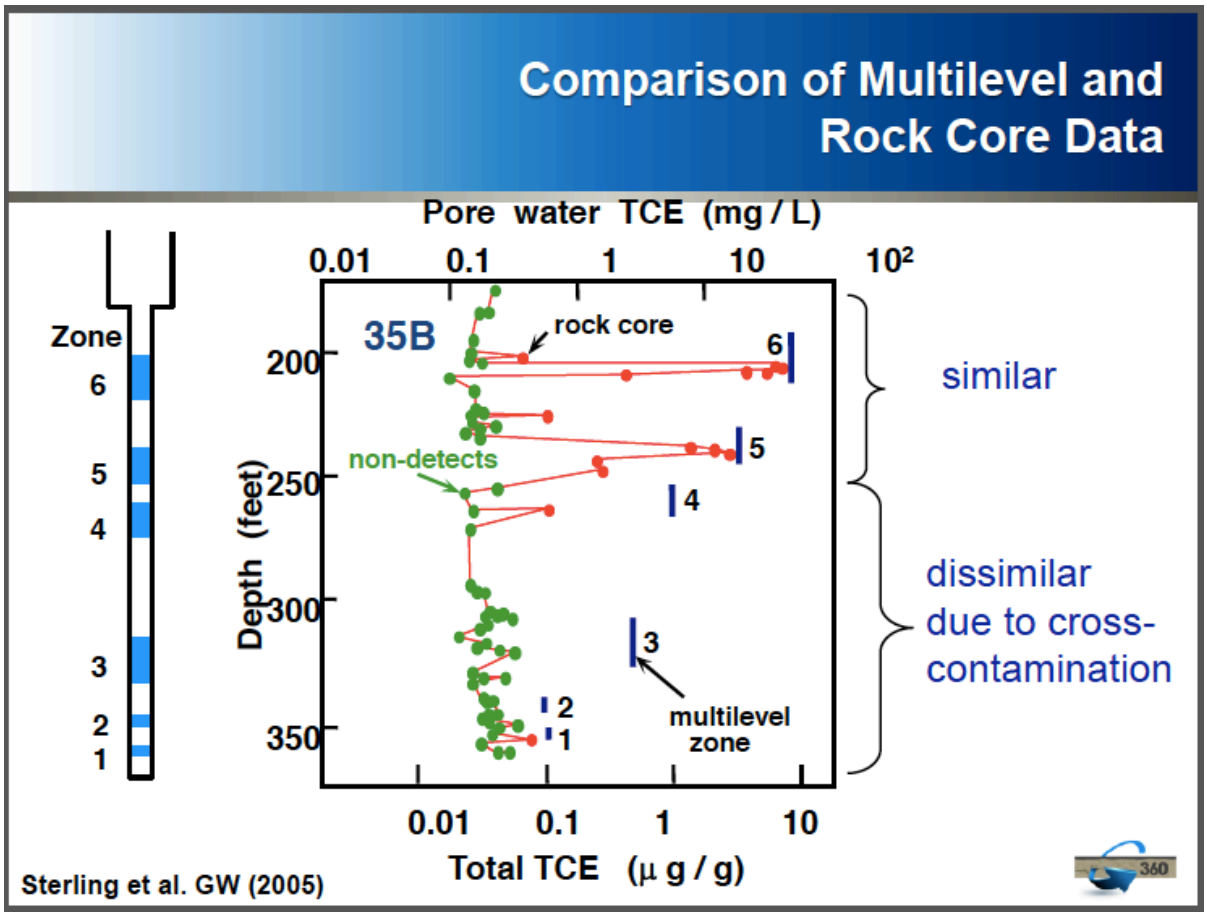

Figure 32 Comparison of Multilevel and Rock Core Data (Parker, 2012)

A numerical model becomes more valuable as it presents more and more information as the "real word". More parameters controlling on architecture such as stratigraphy, fracture network discontinuities, etc. are worth to present on the model. And biodegradation might be taken into consideration in the further study for the degradation products or other contaminants have been found in some off-set seeps or springs at the SSFL (Cherry, McWhorter et al. 2009). Computation technology such as parallel computing and dimension reduction may be helpful to improve the model so as to increase the size of the domain and speed up the simulation.

Bibliography

Abbey, D., P. Martin, et al. (2009). “Simulating Groundwater Flow in a Complex Setting: Development and Application of the Three-Dimensional Mountain-Scale Groundwater Flow Model of the Santa Susana Field Laboratory” SCM Document 3 OF 4.

Amirtharaj, E. S., M. A. Ioannidis, B. Parker, and C. D. Tsakiroglou (2011), Statistical synthesis of imaging and porosimetry data for the characterization of microstructure and transport properties of sandstones, Transport in Porous Media, 86(1), 135–154.

Chapman, S.W., J.A. Cherry, B.L. Parker (2009). “Chlorinated Solvent Plume Front Retardation due to Matrix Diffusion in Fractured Sandstone (Constant Source) .” SCM Document 4 OF 4.

Cherry, J., D. McWhorter, et al. (2009). "Overview of the Site Conceptual Model for the Migration and Fate of Contaminants in Groundwater at the Santa Susana Field Laboratory, Simi, California." SCM Document1 OF 4.

Cherry, J., D. McWhorter, et al. (2009). Site Conceptual Model for the Migration and Fate of Contaminants in Groundwater at the SSFL. SCM Document 0-2: Overview

Goldstein, K.J., A.R. Vitolins, D. Navon, B.L. Parker, S.W. Chapman, and G.A. Anderson. 2004. Characterization and pilot-scale studies for chemical oxidation remediation of fractured shale. Remediation 14, no.4: 19-37.

Hoteit H, Firoozabadi A. An efficient numerical model for incompressible two-phase flow in fractured media. Advances in Water Resources. 2008, June;31(6):891-905.

Howard, P.H. Handbook of Environmental Fate and Exposure Data for Organic Chemicals - Volume II. Solvents (Chelsea, MI: Lewis Publishers, 1991).

Hurley, J.C. 2003. Rock core investigation of DNAPL penetration and persistence in fractured sandstone. Master's thesis, Earth Sciences Department, University of Waterloo.

Hurley, J.C., J.A. Cherry, B.L. Parker (2009). “The Chatsworth Formation underlies most of the SSFL and its matrix porosity provided by interconnected pores is large.” SCM Document 1 OF 4.

Hurley, J.C., J.A. Cherry, B.L. Parker (2009). “TCE DNAPL has been converted to dissolved phase TCE, and this mass has stayed close to home.” SCM Document 4 OF 4.

Hurley, J.C. and Parker, B.L. 2002. Rock core investigation of DNAPL penetration and TCE mobility in fractured sandstone. In: Ground and Water: Theory to Practice, Proceedings of the 55th

Canadian Geotechnical and 3rd Joint IAH-CNC and CGS Groundwater Specialty Conferences. Eds. Stolle D., A.R. Piggott and J.J. Crowder, Southern Ontario Section of the Canadian Geotechnical Society

Kennel, J., J. Meyer, et. al. (2009). "Development of a Storage System for Data from the Discrete Fracture Network (DFN) Approach" SCM Document 1 OF 4.

Lipson, D.S., B.H. Kueper, and M.J. Gefell. 2005. Matrix diffusion-derived plume attenuation in fractured bedrock. Ground Water 43, no.1: 30-39

Narasimhan T. Multidimensional Numerical-Simulation of Fluid-Flow in Fractured Porous-Media. Water Resources Research. 1982;18(4):1235-1247.

Parker, B.L (2009), "The Discrete Fractured Network (DFN) Approach for Characterization of Contaminated Fractured Rock Sites" SCM Document1 OF 4.

Parker, B.L (2012), "Characterization Techniques for Identifying Hydraulically Active Fractures in Sedimentary Rocks" MGWA Spring 2012 Conference Conduits, Karst, and Contamination Addressing Groundwater Challenges

Parker, B.L.,S. Sterling (2009). "A New Method for Measurement of Volatile Organic Contaminants (VOCs) in Rock Core" SCM Document 1 OF 4.

Parker BL, Chapman SW, Cherry JA. Column Theme: Advances and Strategies in Groundwater Remediation. Ground Water. 2010, November-December;48(6):799-803.

Parker BL, Cherry JA, Chapman SW. Discrete Fracture Network Approach for Studying Contamination in Fractured Rock. AQUA mundi. 2012, December;:101-116.

Pehme, P.E., J.P. Greenhouse, and B.L. Parker. 2007. The active line source temperature logging technique and its application in fractured rock hydrogeology. Journal of Environmental & Engineering Geophysics 12, no.4: 307-322.

Reynolds DA, Kueper BH. Multiphase flow and transport through fractured heterogeneous porous media. Journal of Contaminant Hydrology. 2004;71:89-110.

Schwarzenbach, R., P. Gschwend, and D. Imboden, 1993. Environmental Organic Chemistry, JohnWiley and Sons, Inc, New York, USA.

Slough K, Sudicky E, Forsyth P. Grid refinement for modeling multiphase flow in discretely fractured porous media. Advances in Water Resources. 1999, November 1;23(3):261-269.

Slough K, Sudicky E, Forsyth P. Importance of rock matrix entry pressure on DNAPL migration in fractured geologic materials. Ground Water. 1999, March-April;37(2):237-244.

Snow, D.T. 1969. Anisotropic permeability of fractured media. Water Resource Research. V. 5. pp. 1273-1289

Sterling, S.N. 1999. Comparison of Discrete Depth Sampling Using Rock Core and a Removable Multilevel System in a TCE Contaminated Fractured Sandstone. Master's thesis, Earth Sciences Department, University of Waterloo.

Sterling, S.N., B.L. Parker, J.A. Cherry, J.H. Williams, J.W. Lane Jr., and F.P. Haeni. 2005. Vertical cross contamination of trichloroethylene in a borehole in fractured sandstone. Ground Water 43, no.4: 557-573.

Sudicky, E.A. and R.G. McLaren. 1992. The Laplace transform Galerkin technique for large- scale simulation of mass transport in discretely fractured porous formations. Water Resources Research 28, no.2: 499-514.

Unger AJA, Bodvarsson GS, Simmons AM. Simulating infiltration in unsaturated basalt for the Large-Scale Aquifer Pumping and Infiltration Test at INEEL [Simulation de l'infiltration dans des basaltes non-saturş pour des tests à grande échelle de pompage et d'infiltration à l'INEEL]. Journal of Hydraulic Research. 2004;42(Extra Issue):105-113.

Unger, A. and Mase, C. 1993. Numerical study of the hydromechanical behaviour of two rough fracture sur- faces in contact. Water Resources Research 29(7): 2101–2114.

VanderKwaak, J.E. and E.A. Sudicky. 1996. Dissolution of non-aqueous-phase liquids and aqueous-phase contaminant transport in discretely-fractured porous media. Journal of Contaminant Hydrology 23, no.1-2: 45-68.

Walter A. Illman . Hydraulic Tomography Offers Improved Imaging of Heterogeneity in Fractured Rocks. Groundwater 2014; 52: 659.

Walton, K., 2013. On modeling three-phase flow in discretely fractured porous rock. Doctor's thesis, Earth Sciences Department, University of Waterloo.

Walton, K., A. Unger, B.L. Parker and M. Ioannidis. 2011. Simulating infiltration of TCE and water in unsaturated, discretely fractured rock. To be presented at GeoHydro 2011 Water and Earth: The Junction of Quaternary Geoscience and Hydrogeology Conference, Quebec City, QC. August 28-31.

Walton, K., A. Unger, et al. (2012). "Simulating infiltration of TCE and water in unsaturated, discretely fractured rock." GeoHydro 2011 Water and Earth.